Communications in Applied Mathematics and Computational Science

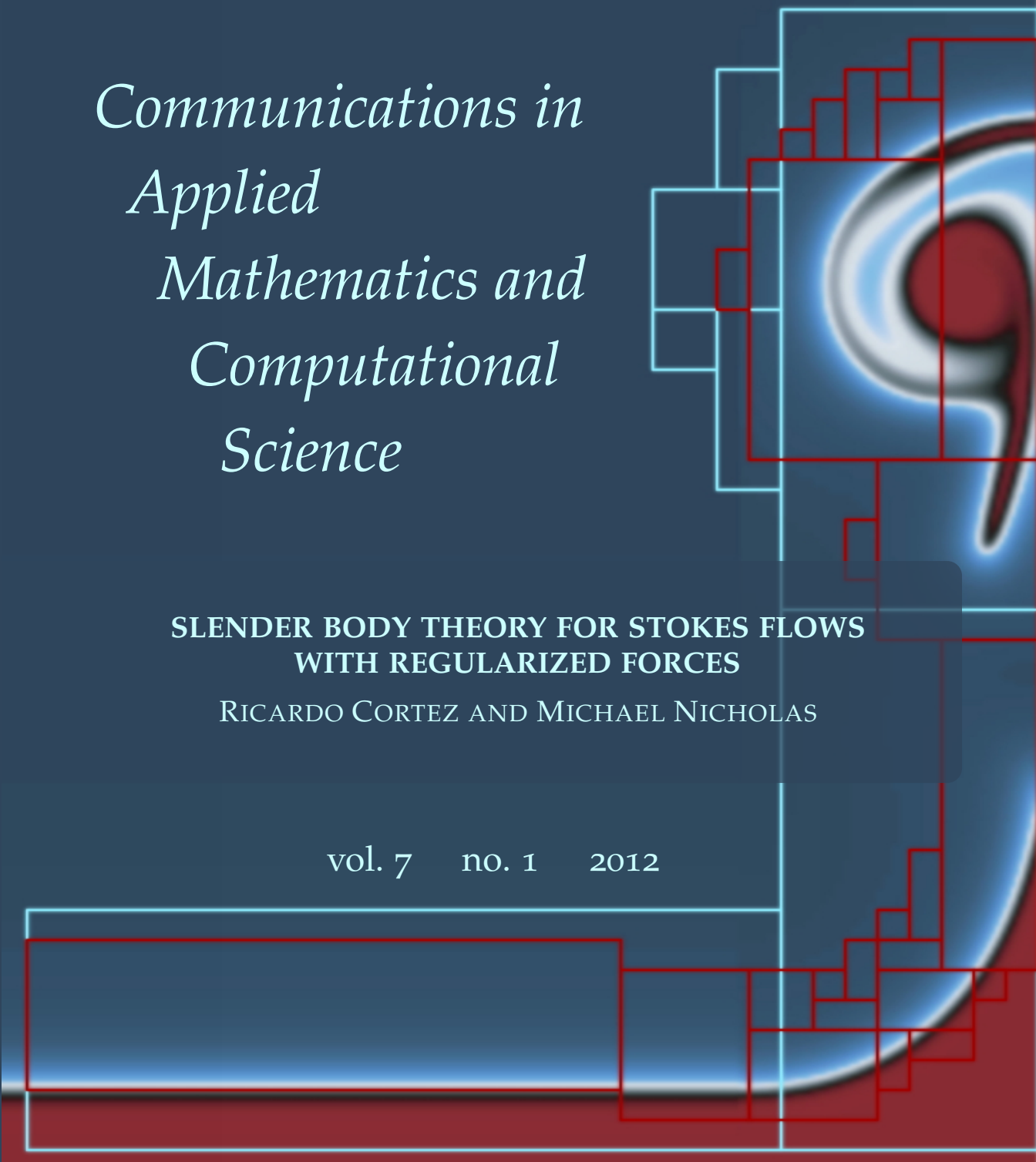

SLENDER BODY THEORY FOR STOKES FLOWS WITH REGULARIZED FORCES

RICARDO CORTEZ AND MICHAEL NICHOLAS

vol. 7 no. 1 2012

mathematical sciences publishers

COMM. APP. MATH. AND COMP. SCI.
Vol. 7, No. 1, 2012

msp

SLENDER BODY THEORY FOR STOKES FLOWS WITH REGULARIZED FORCES

RICARDO CORTEZ AND MICHAEL NICHOLAS

Existing slender body theories for the dynamics of a thin tube in a Stokes flow differ in the way the asymptotic errors depend on a small parameter defined as the radius of the body over its length. Examples are the theory of Lighthill, that of Keller and Rubinow, and that of Johnson. Slender body theory is revisited here in the more general setting of forces which are localized but smoothly varying within a small neighborhood of the filament centerline, rather than delta distributions along the centerline. Physically, this means that the forces are smoothly distributed over the cross-section of the body. The regularity in the forces produces a final expression that has built-in smoothing which helps eliminate instabilities encountered in computations with unsmoothed formulas. Consistency with standard theories is verified in the limit as the smoothing parameter vanishes, where the original expressions are recovered. In addition, an expression for the fluid velocity at locations off the slender body is derived and used to compute the flow around a filament.

1. Introduction

Slender body theories give asymptotic solutions of slender bodies (thin tubular bodies) in a viscous fluid where the small parameter of the expansion is the radius a^* of the tube divided by its length L^*. The goal is to develop an asymptotic formula that relates the velocity of the slender body's surface to forces that are consistent with that motion and are exerted along the centerline (see Figure 1). In our derivation, we nondimensionalize all spatial variables by the length of the tube, L^*, so that $a = a^*/L^*$ is the dimensionless slenderness parameter. In all derivations, the tube dimensionless length is taken to be 1 and we consider a tube with constant circular cross sections (constant a).

Different versions of the theory were developed independently in the 1970's by Lighthill [17] and by Keller and Rubinow [16] using stokeslets and dipole distributions. Johnson developed a slender body theory based on Wu's exact solution of the flow around a spheroidal body (see [13]). Later Johnson [15] made improvements

MSC2000: 76D07, 76Z99.
Keywords: slender body theory, Stokes flow.

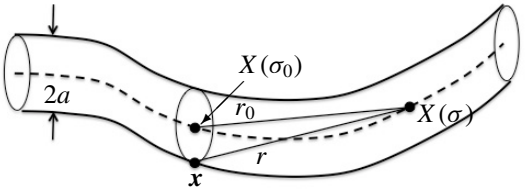

Figure 1. Schematic of a portion of the slender body. All spatial variables are scaled by the tube length so that a is a dimensionless slenderness parameter.

to the theories by adding higher order singularities near the slender body endpoints. Slender body formulations of this type have been used in numerous applications; our focus is on biological ones such as ciliary motion [11; 12], and swimming flagella [13].

The Keller–Rubinow slender body formulation [16] relies on the exact cancellation of integrals that have the same asymptotic singularity. While this is a mathematically elegant formulation, its numerical implementation is unstable to high wave number perturbations [20; 24]. Generally, it is not possible to achieve the same singularity cancellation numerically without problems related to cancellation errors and instability. Roughly speaking, to overcome this problem and stabilize the computation, the integrands in [20; 24] were regularized by replacing r^{-1} with $(r^2+\delta^2)^{-1/2}$ using a clever choice of δ that preserved the order of the asymptotic expansion of the final formula.

In Lighthill's theory [17; 18; 19], a portion of the filament containing the singularity is removed from the integration and replaced with a local term. The remaining integral is no longer singular but care must be taken in the numerical evaluation of it since the kernel has large gradients near the endpoints of the removed piece. A drawback of this formulation is that removing a piece of the integration curve interrupts the periodicity of the problem for a closed filament, eliminating the benefits of the trapezoid rule in periodic domains or the use of spectral methods to approximate the integral.

We address these issues here by re-deriving both theories for the case of force and dipole fields distributed not as delta distributions along the centerline of the body, but distributed over the cross-section of the slender body. This is accomplished by defining a smooth localized spherically symmetric function $\phi_\delta(r)$ (like a narrow Gaussian with standard deviation proportional to the slender body radius) centered at every point $X(s)$ of the body centerline and letting the force be given by $\boldsymbol{F}(\boldsymbol{x}) = \boldsymbol{f}(s)\phi_\delta(|\boldsymbol{x}-X(s)|)$. While the maximum of the force is at the centerline of the slender body, the force is distributed over the entire cross-section of the body, which leads to a regular expression for the velocity of the body. This implies that the regularized Lighthill formulation can be implemented without removing the

piece of the curve where the singularity was. The regularization parameter, δ, is also dimensionless after scaling by the tube length, and is assumed to satisfy $\delta \sim a$.

The solution of the Stokes equations for regularized forces and dipoles is derived in Section 2, including the specific regularizing functions that are used. This solution is used to generate the near-field and far-field expansions for the asymptotic solution. Section 3 contains the derivation of Lighthill's theory for regularized forces and shows that the final expression collapses to Lighthill's formula when the regularization parameter δ vanishes. However, for $\delta > 0$, additional simplifications to the final formula are possible that circumvent the drawbacks discussed above. Section 4 shows the matched asymptotic analysis corresponding to Keller and Rubinow's theory, including simplifications to the final expression for $\delta > 0$. In Section 5 we show validation studies and numerical simulations that compare the two theories both in the case of a closed filament as well as the case of a swimming organism.

2. The flow due to regularized forces

The incompressible Stokes equations in $\mathbb{R}^3$ are

$$\mu \Delta \boldsymbol{u} = \nabla p - \boldsymbol{F}, \tag{1}$$

$$\nabla \cdot \boldsymbol{u} = 0, \tag{2}$$

where μ is the fluid viscosity, $\boldsymbol{u}$ is the fluid velocity, p is the pressure, and $\boldsymbol{F}$ is the body force. The boundary conditions associated with the flow are:

$$\boldsymbol{u}(\boldsymbol{x}) = \boldsymbol{v}(\sigma) \qquad \text{for } \boldsymbol{x} \text{ on the surface of the slender body at cross section } \sigma,$$

$$\boldsymbol{u}(\boldsymbol{x}) \to 0 \qquad \text{as } |\boldsymbol{x}| \to \infty,$$

where $\boldsymbol{v}(\sigma)$ is a translational velocity of the cross section at σ.

Consider the problem in (1)–(2) in the case when the force exerted by the filament on the fluid is given by the function $\boldsymbol{F}(\boldsymbol{x}) = \boldsymbol{f}\ \phi_\delta(\boldsymbol{x})$, where ϕ_δ is a radially symmetric smooth function whose integral over $\mathbb{R}^3$ is 1. For example, ϕ_δ may be a normal density function with standard deviation proportional to the parameter δ. The function ϕ_δ provides the spatial dependence of the body force. The following definitions will be convenient for the derivation of the exact solution of these equations.

Definitions. Let the regularized Green's function $G_\delta(\boldsymbol{x})$ be the free-space solution of $\Delta G_\delta = \phi_\delta$ and let $B_\delta(\boldsymbol{x})$ be the free-space solution of $\Delta B_\delta = G_\delta$.

The function $G_\delta(\boldsymbol{x})$ is a smooth function that is bounded everywhere and closely approximates the Green's function $G(\boldsymbol{x}) = -(4\pi|\boldsymbol{x}|)^{-1}$ for $|\boldsymbol{x}| > \delta$. Similarly $B_\delta(\boldsymbol{x})$ is smooth and approximates $B(\boldsymbol{x}) = -|\boldsymbol{x}|/8\pi$, the solution of the equation $\Delta B(\boldsymbol{x}) = G(\boldsymbol{x})$.

Taking the divergence of (1) and using (2) we have that $\nabla \cdot \boldsymbol{F} = \Delta p$, which gives

$$p(\boldsymbol{x}) = \boldsymbol{f} \cdot \nabla G_\delta(\boldsymbol{x}). \tag{3}$$

The equation for $\boldsymbol{u}$ now becomes $\mu \Delta \boldsymbol{u} = (\boldsymbol{f} \cdot \nabla)\nabla G_\delta - \boldsymbol{f}\ \phi_\delta$, whose particular solution is

$$\mu \boldsymbol{u}(\boldsymbol{x}) = (\boldsymbol{f} \cdot \nabla)\nabla B_\delta(\boldsymbol{x}) - \boldsymbol{f}\ G_\delta(\boldsymbol{x}).$$

This is referred to as *regularized stokeslet* flow. To this particular solution one can add $[\boldsymbol{D}\phi_\delta - (\boldsymbol{D} \cdot \nabla)\nabla G_\delta]$, which represents a regularized dipole flow whose divergence is zero everywhere and is harmonic outside the support of ϕ_δ. In this way we obtain the more general solution

$$\mu \boldsymbol{u}(\boldsymbol{x}) = (\boldsymbol{f} \cdot \nabla)\nabla B_\delta(\boldsymbol{x}) - \boldsymbol{f}\ G_\delta(\boldsymbol{x}) + \boldsymbol{D}\phi_\delta - (\boldsymbol{D} \cdot \nabla)\nabla G_\delta + \mu \boldsymbol{U}, \tag{4}$$

where $\boldsymbol{U}$ is a constant flow that may depend on $\boldsymbol{f}$ and $\boldsymbol{D}$.

Using the fact that G_δ and B_δ are radially symmetric, (4) can be written as

$$8\pi\mu(\boldsymbol{u}(\boldsymbol{x}) - \boldsymbol{U}) = \boldsymbol{f}\ \frac{H_1(|\boldsymbol{x}|)}{|\boldsymbol{x}|} + (\boldsymbol{f} \cdot \boldsymbol{x})\boldsymbol{x}\frac{H_2(|\boldsymbol{x}|)}{|\boldsymbol{x}|^3} - 2\boldsymbol{D}\ \frac{H_3(|\boldsymbol{x}|)}{|\boldsymbol{x}|^3} + 6(\boldsymbol{D} \cdot \boldsymbol{x})\boldsymbol{x}\frac{H_4(|\boldsymbol{x}|)}{|\boldsymbol{x}|^5}$$

where the smoothing functions depend on the blob ϕ_δ. They are defined by the relations

$$H_1(r) = 8\pi\big(B'_\delta(r) - rG_\delta(r)\big), \qquad H_2(r) = 8\pi\big(rB''_\delta(r) - B'_\delta(r)\big),$$
$$H_3(r) = 4\pi r^2\big(G'_\delta(r) - r\phi_\delta(r)\big), \qquad H_4(r) = \tfrac{4}{3}\pi r^2\big(G'_\delta(r) - rG''_\delta(r)\big).$$

One can check that for fixed $\delta > 0$ we have

- $\lim_{r\to\infty} H_k(r) = 1$, for $k = 1, 2, 3, 4$;
- for $r \ll \delta$,

$$H_1(r) = O\Big(\frac{r}{\delta}\Big),\ \ H_2(r) = O\Big(\Big(\frac{r}{\delta}\Big)^3\Big),\ \ H_3(r) = O\Big(\Big(\frac{r}{\delta}\Big)^3\Big),\ \ H_4(r) = O\Big(\Big(\frac{r}{\delta}\Big)^5\Big).$$

The velocity formula has been derived for arbitrary isolated force $\boldsymbol{f}$ and dipole strength $\boldsymbol{D}$. In the case of a filament given by $X(\sigma)$, where σ is the arclength parameter with $0 \le \sigma \le 1$, the velocity at any point $\boldsymbol{x}$ is given by

$$8\pi\mu(\boldsymbol{u}(\boldsymbol{x}) - \boldsymbol{U}) = \int_0^1 \boldsymbol{f}(\sigma)\frac{H_1(r)}{r} + (\boldsymbol{f} \cdot \boldsymbol{r})\boldsymbol{r}\frac{H_2(r)}{r^3} - 2\boldsymbol{D}(\sigma)\frac{H_3(r)}{r^3} + 6(\boldsymbol{D} \cdot \boldsymbol{r})\boldsymbol{r}\frac{H_4(r)}{r^5}\,d\sigma, \tag{5}$$

where $\boldsymbol{r} = \boldsymbol{x} - X(\sigma)$ and $r = |\boldsymbol{r}|$. The constant field $\boldsymbol{U}$ and the dipole strength distribution $\boldsymbol{D}(\sigma)$ give the degrees of freedom needed to enforce boundary conditions at $|\boldsymbol{x}| \to \infty$ and at the filament surface.

2.1. ***Choice of blob function.*** Before proceeding we need to choose the regularizing function. Throughout the paper we will use radially symmetric blobs with infinite support. It turns out to be convenient (although not necessary) to choose one regularization for the stokeslets and a different one for the dipoles [1] in order to achieve simplified expressions. Using

$$\phi_\delta(r) = \frac{15\delta^4}{8\pi(r^2+\delta^2)^{7/2}} \quad \text{and} \quad \psi(r) = \frac{3\delta^2}{4\pi(r^2+\delta^2)^{5/2}}, \tag{6}$$

for the stokeslets and dipoles, respectively, the functions in (5) are

$$\begin{aligned} H_1(r) &= r\left(\frac{1}{\sqrt{r^2+\delta^2}} + \frac{\delta^2}{(r^2+\delta^2)^{3/2}}\right), & H_2(r) &= r\left(\frac{1}{\sqrt{r^2+\delta^2}} - \frac{\delta^2}{(r^2+\delta^2)^{3/2}}\right), \\ H_3(r) &= r^3\left(\frac{1}{(r^2+\delta^2)^{3/2}} - \frac{3\delta^2}{(r^2+\delta^2)^{5/2}}\right), & H_4(r) &= \frac{r^5}{(r^2+\delta^2)^{5/2}} \end{aligned} \tag{7}$$

and are shown in Figure 2. Other choices of regularization are possible, including Gaussians and functions with compact support. In all cases, the regularization parameter δ is chosen to be $\delta = O(a)$.

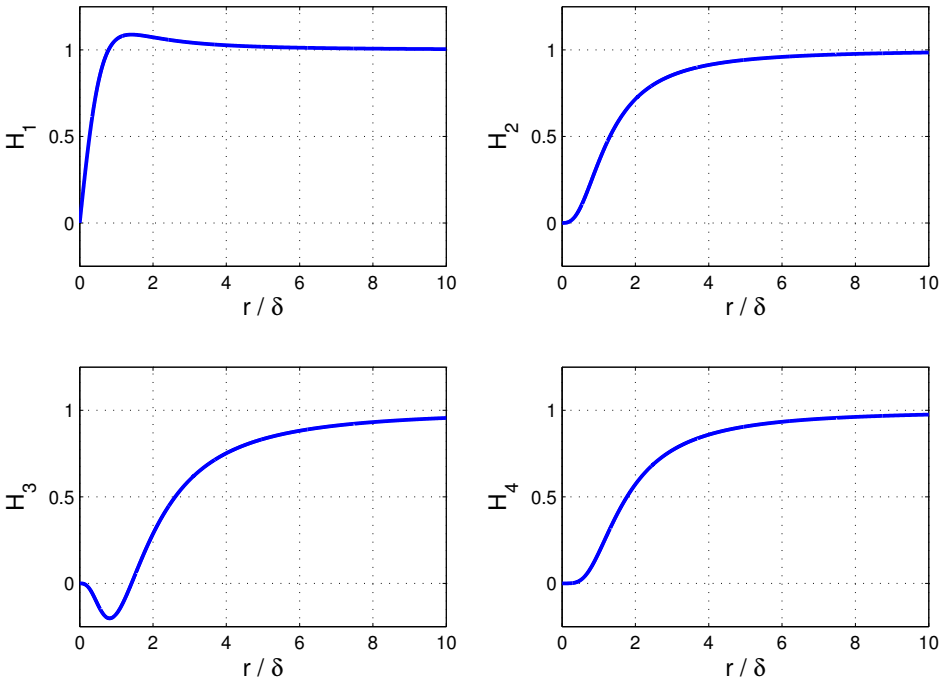

Figure 2. Graphs of the smoothing functions H_1–H_4 as functions of r/δ.

3. Lighthill's theory

We consider first a construction of the slender body velocity following the strategy in [17; 18; 19]. In Lighthill's theory, it is sufficient to choose the constant flow $\boldsymbol{U} = \boldsymbol{0}$ and to consider the evaluation of the velocity at a point $\boldsymbol{x}$ on the surface of the slender body. The velocity is given by (5):

$$8\pi\mu\boldsymbol{u}(\boldsymbol{x}) = \int_0^1 \boldsymbol{f}(\sigma)\frac{H_1(r)}{r} + (\boldsymbol{f}\cdot\boldsymbol{r})\boldsymbol{r}\frac{H_2(r)}{r^3} - 2\boldsymbol{D}(\sigma)\frac{H_3(r)}{r^3} + 6(\boldsymbol{D}\cdot\boldsymbol{r})\boldsymbol{r}\frac{H_4(r)}{r^5}\,d\sigma,$$

where $\boldsymbol{r} = \boldsymbol{x} - X(\sigma)$.

Specifically, consider the integral evaluated on the surface of the cross-section at $\sigma = \sigma_0$ and select an intermediate length scale represented by q with $a \ll q \ll 1$ and make the following assumptions:

(1) q is large enough that for $r > q$, the dipole contribution is negligible due to the high singularity, and the stokeslet contribution does not vary significantly on the cross-section at σ_0.

(2) q is small enough that the portion of the slender body corresponding to $|\sigma - \sigma_0| < q$ is straight (has zero curvature), and $\boldsymbol{f}(\sigma)$ and $\boldsymbol{D}(\sigma)$ do not vary significantly from their values at σ_0.

Although the velocity formula above is evaluated at a point $\boldsymbol{x}$ on the surface of the slender body, the goal is to reduce this formula to one that is evaluated at the centerline point $X(\sigma_0)$, corresponding to the center of the cross-section containing $\boldsymbol{x}$. The result would be an expression involving only centerline points but consistent with the correct boundary conditions on the surface of the slender body. The velocity expression will be separated into two pieces: the near field corresponding to $|\sigma - \sigma_0| < q$ and the far field. The first assumption will be used to simplify the far field and the second one to simplify the near field.

Let $\hat{\boldsymbol{b}}$ be a unit vector normal to the centerline at $X(\sigma_0)$ and write (see Figure 1)

$$\boldsymbol{x} = X(\sigma_0) + a\hat{\boldsymbol{b}}, \quad \boldsymbol{r}_0 = X(\sigma_0) - X(\sigma), \quad \boldsymbol{r} = \boldsymbol{x} - X(\sigma).$$

3.1. ***The far field.*** The far field is expressed as

$$\int_{|\boldsymbol{r}|>q} \boldsymbol{f}(\sigma)\frac{H_1(r)}{r} + (\boldsymbol{f}\cdot\boldsymbol{r})\boldsymbol{r}\frac{H_2(r)}{r^3} - 2\boldsymbol{D}(\sigma)\frac{H_3(r)}{r^3} + 6(\boldsymbol{D}\cdot\boldsymbol{r})\boldsymbol{r}\frac{H_4(r)}{r^5}d\sigma.$$

In the far field, the dipole contribution is insignificant and the stokeslet contribution is independent of the evaluation point on the cross-section centered at $X(\sigma_0)$. Consequently, one choose $\boldsymbol{D} = 0$ and $\boldsymbol{r} = \boldsymbol{r}_0$ in the integral above to get

$$8\pi\mu\boldsymbol{u}_{far}(\sigma_0) = \int_{|\boldsymbol{r}_0|>q} \boldsymbol{f}(\sigma)\frac{H_1(r_0)}{r_0} + (\boldsymbol{f}\cdot\boldsymbol{r}_0)\boldsymbol{r}_0\frac{H_2(r_0)}{r_0^3}d\sigma + O(a). \qquad (8)$$

The error term in this equation is due to the fact that

$$(\boldsymbol{f}\cdot\boldsymbol{r})\boldsymbol{r} = (\boldsymbol{f}_0\cdot\boldsymbol{r}_0)\boldsymbol{r}_0 + a[(\boldsymbol{f}_0\cdot\hat{\boldsymbol{b}})\boldsymbol{r}_0 + (\boldsymbol{f}_0\cdot\boldsymbol{r}_0)\hat{\boldsymbol{b}}] + a^2(\boldsymbol{f}_0\cdot\hat{\boldsymbol{b}})\hat{\boldsymbol{b}}. \tag{9}$$

and that in the far field of point $X(\sigma_0)$ the shape of the slender body is arbitrary so there is no reason to expect any cancellation from symmetries.

3.2. ***The near field.*** Now, the near-field contribution is given by

$$8\pi\mu\boldsymbol{u}_{\text{near}}(\sigma_0) = \int_{|\boldsymbol{r}|<q} \boldsymbol{f}(\sigma)\frac{H_1(r)}{r} + (\boldsymbol{f}\cdot\boldsymbol{r})\boldsymbol{r}\frac{H_2(r)}{r^3} - 2\boldsymbol{D}(\sigma)\frac{H_3(r)}{r^3} + 6(\boldsymbol{D}\cdot\boldsymbol{r})\boldsymbol{r}\frac{H_4(r)}{r^5}\,d\sigma.$$

We consider q small enough that the force does not vary significantly from $\boldsymbol{f}(\sigma_0)$ and the dipole strength does not vary significantly from $\boldsymbol{D}(\sigma_0)$. Then for a straight filament, the vector $\boldsymbol{r}_0 = (\sigma_0 - \sigma)\boldsymbol{s}$ is an odd function, so that the term proportional to a in (9) will provide no contribution to the integral. We are left with

$$8\pi\mu\boldsymbol{u}_{\text{near}}(\sigma_0) = \int_{|\boldsymbol{r}|<q}\Bigg(\boldsymbol{f}_0\frac{H_1(r)}{r} + \big((\boldsymbol{f}_0\cdot\boldsymbol{r}_0)\boldsymbol{r}_0 + a^2(\boldsymbol{f}_0\cdot\hat{\boldsymbol{b}})\hat{\boldsymbol{b}}\big)\frac{H_2(r)}{r^3} - 2\boldsymbol{D}_0\frac{H_3(r)}{r^3} + 6\big((\boldsymbol{D}_0\cdot\boldsymbol{r}_0)\boldsymbol{r}_0 + a^2(\boldsymbol{D}_0\cdot\hat{\boldsymbol{b}})\hat{\boldsymbol{b}}\big)\frac{H_4(r)}{r^5}\Bigg)\,d\sigma.$$

In order for the entire cross-section of the filament at σ_0 to move with the same velocity, the integral cannot depend on the vector $\hat{\boldsymbol{b}}$, which is a unit vector normal to the filament at σ_0 but otherwise arbitrary. We therefore enforce the condition that

$$\int_{|\boldsymbol{r}|<q} (\boldsymbol{f}_0\cdot\hat{\boldsymbol{b}})\hat{\boldsymbol{b}}\,\frac{H_2(r)}{r^3} + 6(\boldsymbol{D}_0\cdot\hat{\boldsymbol{b}})\hat{\boldsymbol{b}}\,\frac{H_4(r)}{r^5}d\sigma = 0,$$

which is used to determine the strength of the dipole $\boldsymbol{D}_0$ as a function of $\boldsymbol{f}_0$. This approach is exactly analogous to the problem of a sphere moving at constant velocity in a Stokes fluid. A single stokeslet at the center of the sphere is not sufficient to provide the correct velocity, but a stokeslet plus a dipole at the center will suffice, provided the dipole strength is related to the stokeslet strength in a way that cancels the dependence on the evaluation point on the surface [2].

Computing the last integral exactly and neglecting terms containing $O(a^2/q^2)$ and $O(\delta^2/q^2)$, we have that

$$\frac{2}{(a^2+\delta^2)}(\boldsymbol{f}_0\cdot\hat{\boldsymbol{b}})\hat{\boldsymbol{b}} + \frac{8}{(a^2+\delta^2)^2}(\boldsymbol{D}_0\cdot\hat{\boldsymbol{b}})\hat{\boldsymbol{b}} = 0$$

from which we deduce that

$$\boldsymbol{D}_0 = -\frac{a^2+\delta^2}{4}\,\boldsymbol{f}_n, \tag{10}$$

where $\boldsymbol{f}_n := \boldsymbol{f}_0 - (\boldsymbol{f}_0 \cdot \boldsymbol{s})\boldsymbol{s}$represents the component of $\boldsymbol{f}_0$ normal to the filament. Note that the dipole strength is strictly normal to the filament; it does not have a tangential component.

The near-field velocity is thus given by

$$8\pi\mu \boldsymbol{u}_{\text{near}}(\sigma_0) = \int_{|\boldsymbol{r}|<q} \boldsymbol{f}_0 \frac{H_1(r)}{r} + (\boldsymbol{f}_0 \cdot \boldsymbol{r}_0)\boldsymbol{r}_0 \frac{H_2(r)}{r^3} - 2\boldsymbol{D}_0 \frac{H_3(r)}{r^3} + 6(\boldsymbol{D}_0 \cdot \boldsymbol{r}_0)\boldsymbol{r}_0 \frac{H_4(r)}{r^5}\, d\sigma.$$

Before proceeding, we decompose the force into its normal and tangential components, $\boldsymbol{f}_0 = \boldsymbol{f}_n + \boldsymbol{f}_\tau$, and note that to leading order, $\boldsymbol{r}_0 = (\sigma_0 - \sigma)\boldsymbol{s}$, so that $(\boldsymbol{f}_0 \cdot \boldsymbol{r}_0)\boldsymbol{r}_0 = (\sigma - \sigma_0)^2 \boldsymbol{f}_\tau$. Using (10), we get

$$8\pi\mu \boldsymbol{u}_{\text{near}}(\sigma_0) = 2(\boldsymbol{f}_n + 2\boldsymbol{f}_\tau)\left[\ln\frac{2q}{\beta} - \frac{a^2}{2\beta^2}\right] + 2\boldsymbol{f}_n\left[1 - \frac{\delta^2}{2\beta^2}\right] + O(\epsilon^2), \quad (11)$$

where we have defined $\beta^2 = a^2 + \delta^2$ and $\epsilon = \max(a/q, \delta/q)$.

At this point, one can combine (8) and (11) to get the velocity. However, there is something unattractive about these expressions: they depend on a choice of q. But aside from some scaling requirements, q is arbitrary.

Lighthill devised a way to eliminate this ambiguity in a way that can be adjusted to the present context. Since the far field is simply the integral of the stokeslet field, we compute to leading order for any number θ satisfying $0 < \theta < q$,

$$\int_{\theta<r_0<q} \boldsymbol{f}_0 \frac{H_1(r_0)}{r_0} + (\boldsymbol{f}_0 \cdot \boldsymbol{r}_0)\boldsymbol{r}_0 \frac{H_2(r_0)}{r_0^3}\, d\sigma = 2(\boldsymbol{f}_n + 2\boldsymbol{f}_\tau)\ln\frac{2q}{\theta + \sqrt{\theta^2+\delta^2}} + 2\boldsymbol{f}_n\left[1 - \frac{\theta}{\sqrt{\theta^2+\delta^2}}\right]$$

and since (11) can be written as

$$8\pi\mu \boldsymbol{u}_{\text{near}}(\sigma_0) = 2(\boldsymbol{f}_n + 2\boldsymbol{f}_\tau)\ln\frac{2q}{\beta e^{a^2/2\beta^2}} + 2\boldsymbol{f}_n\left[1 - \frac{\delta^2}{2\beta^2}\right],$$

we can define the number θ by making the identification

$$\theta + \sqrt{\theta^2+\delta^2} = \beta e^{a^2/2\beta^2},$$

so that

$$8\pi\mu \boldsymbol{u}_{\text{near}}(\sigma_0) = 2\boldsymbol{f}_n\left[\frac{\theta}{\sqrt{\theta^2+\delta^2}} - \frac{\delta^2}{2\beta^2}\right] + \int_{\theta<r_0<q} \boldsymbol{f}_0 \frac{H_1(r_0)}{r_0} + (\boldsymbol{f}_0 \cdot \boldsymbol{r}_0)\boldsymbol{r}_0 \frac{H_2(r_0)}{r_0^3}\, d\sigma.$$

By writing the near field in this way and adding it to the far field in (8), we get a final expression which is independent of q:

$$8\pi\mu\boldsymbol{u}(\sigma_0) = 2\boldsymbol{f}_n\left[1 - \frac{2\delta^2}{\beta^2 e^{a^2/\beta^2} + \delta^2} - \frac{\delta^2}{2\beta^2}\right] + \int_{\theta<r_0} \boldsymbol{f}(\sigma)\frac{H_1(r_0)}{r_0} + (\boldsymbol{f}\cdot\boldsymbol{r}_0)\boldsymbol{r}_0\frac{H_2(r_0)}{r_0^3}\,d\sigma, \quad (12)$$

where $\boldsymbol{r}_0 = X(\sigma_0) - X(\sigma)$, $r_0 = |\boldsymbol{r}_0|$, $\beta^2 = a^2 + \delta^2$, and

$$\theta = \frac{1}{2\beta}\left(\beta^2 e^{a^2/2\beta^2} - \delta^2 e^{-a^2/2\beta^2}\right).$$

Formula (12) indicates that the velocity of the filament at $X(\sigma_0)$ has two contributions. One is the integral of the regularized stokeslet field evaluated at the centerline, with the portion $|\sigma - \sigma_0| < \theta$ excluded. The other one is a local term proportional to the component of force normal to the filament at σ_0.

3.3. ***The limit $\delta \to 0$.*** Notice that as the regularization δ vanishes, we have that $\beta \to a$ and therefore $\theta \to \theta_0 = a\sqrt{e}/2 \approx 0.824a$. In this limit, $H_1(r) \to 1$, $H_2(r) \to 1$ and the local term reduces to $2\boldsymbol{f}_n$, so that the entire expression for velocity is in agreement with Lighthill's basic theorem of flagellar hydrodynamics [18; 19]. The expression derived here is therefore more general since it includes the previously developed case of delta force distributions and extends it to the case of regular forces distributed over the body's cross-section. Figure 3 shows the relative size of the bracketed expression in the local term of (12) and of the parameter θ as functions of the regularization parameter δ.

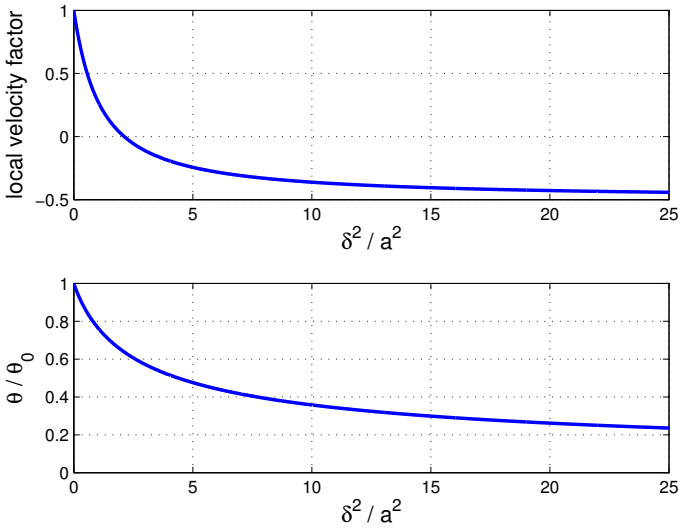

Figure 3. Graphs of the bracketed factor in the local term of the velocity in (12) and $\theta/\theta_0 = 2\theta/a\sqrt{e}$ as functions of δ^2/a^2.

3.4. ***Simplifications for $\delta > 0$.*** In the case $\delta = 0$, the excluded part of the integral in (12) is necessary because the stokeslet field is not integrable in any neighborhood of σ_0. For a closed filament, spectral methods are efficient numerical techniques for computing the integral accurately; however, the missing piece of the integral gets in the way of an efficient implementation of such methods. However, in the regularized case (when $\delta > 0$), the velocity expression is integrable and one can write it as the integral from $\sigma = 0$ to $\sigma = 1$ by simply adding and subtracting the excluded piece. By assumption in the region $|\sigma - \sigma_0| < \theta$, the force is considered constant: $\boldsymbol{f}(\sigma) = \boldsymbol{f}_0$ and $(\boldsymbol{f} \cdot \boldsymbol{r}_0)\boldsymbol{r}_0 = r_0^2\ \boldsymbol{f}_\tau$. After some simplification we have

$$8\pi\mu\boldsymbol{u}(\sigma_0) = 2\boldsymbol{f}_n\left[1 - \frac{\delta^2}{2\beta^2}\right] - (\boldsymbol{f}_n + 2\boldsymbol{f}_\tau)\left[2\ln(\beta/\delta) + 1 - \frac{\delta^2}{\beta^2}\right] + \int_0^1 \frac{\boldsymbol{f}(\sigma)}{\sqrt{r_0^2 + \delta^2}} + \frac{(\boldsymbol{f} \cdot \boldsymbol{r}_0)\boldsymbol{r}_0}{r_0^2\sqrt{r_0^2 + \delta^2}}\, d\sigma, \quad (13)$$

where $\boldsymbol{r}_0 = X(\sigma_0) - X(\sigma)$, $r_0 = |\boldsymbol{r}_0|$, and $\beta^2 = a^2 + \delta^2$.

This formula shows that the integral is that of the standard stokeslet but with the singular factor $1/r$ replaced by $1/\sqrt{r^2 + \delta^2}$. The regularization of the forces is also expected to impact the local terms in the velocity since it is in a neighborhood of the centerline where the forces are most significantly changed. The final formula shows the appropriate form of the local terms in order for the velocity to be consistent with these forces.

4. Keller–Rubinow theory

Lighthill's slender body theory is developed in such a way that the errors depend linearly on the body radius. Keller and Rubinow's theory [16] develops the relationship between velocity and force with errors $O(a^2 \ln a)$ in regions away from the endpoints. In order to achieve this improvement, the near-field and far-field flows are evaluated at fluid locations rather than at a point on the slender body surface. The two expressions are then matched asymptotically at an intermediate distance. In this section, it will be convenient to start with (5) and set the dipole strength equal to a multiple of the force, $\boldsymbol{D} = A\boldsymbol{f}$.

4.1. ***The far field.*** Let $\boldsymbol{x}$ be a point in the fluid far from the slender body. For the far field solution we consider a flow which decays to zero as $|\boldsymbol{x}| \to \infty$. In this case it is possible to choose $A = 0$ and $\boldsymbol{U} = \boldsymbol{0}$ to get

$$8\pi\mu\boldsymbol{u}(\boldsymbol{x}) = \int_0^1 \boldsymbol{f}(\sigma)\ \frac{H_1(r)}{r} + (\boldsymbol{f}(\sigma) \cdot \boldsymbol{r})\boldsymbol{r}\ \frac{H_2(r)}{r^3}\, d\sigma \quad (14)$$

where $\boldsymbol{r} = \boldsymbol{x} - X(\sigma)$ and $r = |\boldsymbol{r}|$.

4.2. ***The near field.*** We now consider a point $\boldsymbol{x}_0$ in the fluid so close to the slender body that the latter can be viewed as a long, thin, straight cylinder of radius a. Without loss of generality we assume that it extends in the $\hat{\boldsymbol{z}}$ direction from $z=-q$ to $z=q$ and that the evaluation point is given by

$$\boldsymbol{x}_0 = (x, y, 0),$$

with $|\boldsymbol{x}_0| = \rho \ll q$. The forces acting along the straight tube are assumed to be constant and equal to $\boldsymbol{f}_0$. Then the velocity at $\boldsymbol{x}_0$ satisfies

$$8\pi\mu(\boldsymbol{u}(\boldsymbol{x}_0) - \boldsymbol{U}) = \int_{-q}^{q} \boldsymbol{f}_0\left(\frac{H_1(|\boldsymbol{y}|)}{|\boldsymbol{y}|} - \frac{2AH_3(|\boldsymbol{y}|)}{|\boldsymbol{y}|^3}\right) + (\boldsymbol{f}_0\cdot\boldsymbol{y})\boldsymbol{y}\left(\frac{H_2(|\boldsymbol{y}|)}{|\boldsymbol{y}|^3} + \frac{6AH_4(|\boldsymbol{y}|)}{|\boldsymbol{y}|^5}\right) dz, \quad (15)$$

where

$$\boldsymbol{y} = \boldsymbol{x}_0 - (0, 0, z) = (x, y, -z).$$

In order to simplify the notation, let $\boldsymbol{s}$ be a unit vector in the positive $\hat{\boldsymbol{z}}$ direction (tangent to the filament). Then

$$(\boldsymbol{f}_0\cdot\boldsymbol{y})\boldsymbol{y} = (\boldsymbol{f}_0\cdot\boldsymbol{x}_0)\,\boldsymbol{x}_0 - z\,[(\boldsymbol{f}_0\cdot\boldsymbol{x}_0)\,\boldsymbol{s} + (\boldsymbol{f}_0\cdot\boldsymbol{s})\,\boldsymbol{x}_0] + z^2(\boldsymbol{f}_0\cdot\boldsymbol{s})\boldsymbol{s}.$$

Using the specific form of the functions $H_1(r)$–$H_4(r)$ in (7), we find that the inner velocity is given by (see Appendix A):

$$\begin{aligned} 8\pi\mu(\boldsymbol{u}(\boldsymbol{x}_0) - \boldsymbol{U}) = \boldsymbol{f}&\left[\ln\frac{4q^2}{|\boldsymbol{x}_0|^2+\delta^2} + \frac{2\delta^2}{|\boldsymbol{x}_0|^2+\delta^2} - 2A\left(\frac{2|\boldsymbol{x}_0|^2-\delta^2}{(|\boldsymbol{x}_0|^2+\delta^2)^2} - \frac{1}{q^2}\right)\right] \\ &+ (\boldsymbol{f}\cdot\boldsymbol{x}_0)\boldsymbol{x}_0\left[\frac{2}{|\boldsymbol{x}_0|^2+\delta^2} + 6A\frac{4}{3(|\boldsymbol{x}_0|^2+\delta^2)^2}\right] \\ &+ (\boldsymbol{f}\cdot\boldsymbol{s})\boldsymbol{s}\left[\ln\frac{4q^2}{|\boldsymbol{x}_0|^2+\delta^2} - 2 + 6A\left(\frac{2}{3(|\boldsymbol{x}_0|^2+\delta^2)} - \frac{1}{q^2}\right)\right]. \end{aligned}$$

4.2.1. *No-slip boundary condition.* We consider the slender body velocity given by the unknown $\boldsymbol{v}(\sigma_0)$. The goal is to develop an expression for $\boldsymbol{v}(\sigma_0)$. The near-field boundary condition must be consistent with a uniform velocity at every point of a cross-section of the slender body. Then we must impose the condition $\boldsymbol{u}(\boldsymbol{x}_0) = \boldsymbol{v}(\sigma_0)$ for all $\boldsymbol{x}_0$ with magnitude $\rho = a$ (i.e. on the surface of the slender body). For this we notice that the second term on the right side of the last equation is the only one that is not radially symmetric. This leads us to choose

$$A = -\frac{a^2+\delta^2}{4}.$$

With this value of A we can solve for the constant flow $\boldsymbol{U}$ in terms of $\boldsymbol{v}(\sigma_0)$ and substitute it back. The final inner velocity expression at a point $\boldsymbol{x}_0$ in the fluid is

$$
\begin{aligned}
&8\pi\mu\boldsymbol{u}(\boldsymbol{x}_0)\\
&= 8\pi\mu\boldsymbol{v}(\sigma_0) - (\boldsymbol{f}_0 + (\boldsymbol{f}_0\cdot\boldsymbol{s})\boldsymbol{s})\left(\ln\frac{|\boldsymbol{x}_0|^2+\delta^2}{a^2+\delta^2} + \frac{(|\boldsymbol{x}_0|^2-\delta^2)(|\boldsymbol{x}_0|^2-a^2)}{(|\boldsymbol{x}_0|^2+\delta^2)^2}\right)\\
&\qquad + 2(\boldsymbol{f}_0\cdot\boldsymbol{s})\boldsymbol{s}\frac{|\boldsymbol{x}_0|^2(|\boldsymbol{x}_0|^2-a^2)}{(|\boldsymbol{x}_0|^2+\delta^2)^2} + 2(\boldsymbol{f}_0\cdot\boldsymbol{x}_0)\boldsymbol{x}_0\frac{|\boldsymbol{x}_0|^2-a^2}{(|\boldsymbol{x}_0|^2+\delta^2)^2}. \qquad (16)
\end{aligned}
$$

4.3. ***Matching.*** The fluid velocity obtained from the inner expansion (16) is bounded as the filament is approached, i.e., as $|\boldsymbol{x}_0|\to a$. However, it grows logarithmically as $|\boldsymbol{x}_0|$ increases. The outer expansion velocity given by (14) also has a logarithmic term as $\boldsymbol{x}$ approaches a point $X(\sigma_0)$ on the filament. To match the solutions at an intermediate distance, let $\boldsymbol{x}_0 = \boldsymbol{x} - X(\sigma_0)$ with $|\boldsymbol{x}_0| = \rho$ and assume $\delta \sim a \ll \rho \ll 1$. Here $X(\sigma_0)$ is the point on the filament which is closest to $\boldsymbol{x}$ and $\boldsymbol{s}$ is the unit tangent at $X(\sigma_0)$. Then dropping the higher order terms in $O(a^2/\rho^2)$ and $O(\delta^2/\rho^2)$, the inner expansion becomes

$$
\begin{aligned}
&8\pi\mu\boldsymbol{u}(\boldsymbol{x})\\
&\qquad = 8\pi\mu\boldsymbol{v}(\sigma_0) - (\boldsymbol{f}_0 + (\boldsymbol{f}_0\cdot\boldsymbol{s})\boldsymbol{s})\left[\ln\frac{\rho^2+\delta^2}{a^2+\delta^2}+1\right] + 2(\boldsymbol{f}_0\cdot\boldsymbol{s})\boldsymbol{s} + \frac{2(\boldsymbol{f}_0\cdot\boldsymbol{x}_0)\boldsymbol{x}_0}{\rho^2}.
\end{aligned}
$$

The outer expansion velocity is given by (14), which we rewrite as

$$
8\pi\mu\boldsymbol{u}(\boldsymbol{x}) = \int_0^1 J(\boldsymbol{r},\,\rho,\,\delta,\,\boldsymbol{f}(\sigma))\,d\sigma, \qquad (17)
$$

where $\boldsymbol{r} = \boldsymbol{x} - X(\sigma)$. Setting the two expressions equal to each other we get

$$
\begin{aligned}
&\int_0^1 J(\boldsymbol{r},\,\rho,\,\delta,\,\boldsymbol{f}(\sigma))\,d\sigma\\
&\qquad = 8\pi\mu\boldsymbol{v}(\sigma_0) - (\boldsymbol{f}_0 + (\boldsymbol{f}_0\cdot\boldsymbol{s})\boldsymbol{s})\left[\ln\frac{\rho^2+\delta^2}{a^2+\delta^2}+1\right] + 2(\boldsymbol{f}_0\cdot\boldsymbol{s})\boldsymbol{s} + \frac{2(\boldsymbol{f}_0\cdot\boldsymbol{x}_0)\boldsymbol{x}_0}{\rho^2}.
\end{aligned}
$$

The inner expansion of the far field is found by expanding the left-hand side of this equation in powers of ρ (see Appendix B). This yields

$$
\begin{aligned}
&\int_0^1\left(J(\boldsymbol{r}_0,\,0,\,\delta,\,\boldsymbol{f}(\sigma)) - \boldsymbol{f}_0\frac{H_1(|\sigma-\sigma_0|)}{|\sigma-\sigma_0|} - (\boldsymbol{f}_0\cdot\boldsymbol{s})\boldsymbol{s}\frac{H_2(|\sigma-\sigma_0|)}{|\sigma-\sigma_0|}\right)d\sigma \qquad (18)\\
&\quad + (\boldsymbol{f}_0 + (\boldsymbol{f}_0\cdot\boldsymbol{s})\boldsymbol{s})\big[\ln(4\sigma_0(1-\sigma_0)) - \ln(\rho^2+\delta^2)\big] - 2(\boldsymbol{f}_0\cdot\boldsymbol{s})\boldsymbol{s} + \frac{2(\boldsymbol{f}_0\cdot\boldsymbol{x}_0)\boldsymbol{x}_0}{\rho^2}\\
&\qquad = 8\pi\mu\boldsymbol{v}(\sigma_0) - (\boldsymbol{f}_0 + (\boldsymbol{f}_0\cdot\boldsymbol{s})\boldsymbol{s})\left[\ln\frac{\rho^2+\delta^2}{a^2+\delta^2}+1\right] + 2(\boldsymbol{f}_0\cdot\boldsymbol{s})\boldsymbol{s} + \frac{2(\boldsymbol{f}_0\cdot\boldsymbol{x}_0)\boldsymbol{x}_0}{\rho^2},
\end{aligned}
$$

where $\boldsymbol{r}_0 = X(\sigma_0) - X(\sigma)$.

Since $\boldsymbol{x}_0$ is an arbitrary point where the asymptotic matching is done, the final result should not depend on it (or on its magnitude ρ). Fortunately all the terms

containing ρ cancel out of the last equation so that the change of variables $t = \sigma - \sigma_0$ gives

$$8\pi\mu \boldsymbol{v}(\sigma_0) = \int_{-\sigma_0}^{1-\sigma_0} \Bigg(\frac{\boldsymbol{f}(\sigma_0+t)\ H_1(r_0)}{r_0} - \frac{\boldsymbol{f}_0\ H_1(|t|)}{|t|} + \frac{(\boldsymbol{f}(\sigma_0+t)\cdot \boldsymbol{r}_0)\boldsymbol{r}_0\ H_2(r_0)}{r_0^3} - \frac{(\boldsymbol{f}_0\cdot \boldsymbol{s})\boldsymbol{s}\ H_2(|t|)}{|t|} \Bigg) dt + (\boldsymbol{f}_0 + (\boldsymbol{f}_0\cdot \boldsymbol{s})\boldsymbol{s}) \big[\ln(4\sigma_0(1-\sigma_0)) - \ln\left(a^2+\delta^2\right) + 1 \big] - 4(\boldsymbol{f}_0\cdot \boldsymbol{s})\boldsymbol{s}. \quad (19)$$

Our velocity formula can be simplified using the functions H_1–H_4 in (7) (see Appendix C) so that up to $O(\delta^2 \ln \delta)$ the final expression for the filament velocity becomes

$$8\pi\mu \boldsymbol{v}(\sigma_0) = \int_{-\sigma_0}^{1-\sigma_0} \frac{\boldsymbol{f}(\sigma_0+t)}{\sqrt{r_0^2+\delta^2}} + \frac{(\boldsymbol{f}(\sigma_0+t)\cdot \boldsymbol{r}_0)\boldsymbol{r}_0}{r_0^2\sqrt{r_0^2+\delta^2}} - \frac{\boldsymbol{f}_0 + (\boldsymbol{f}_0\cdot \boldsymbol{s})\boldsymbol{s}}{\sqrt{t^2+\delta^2}}\, dt + (\boldsymbol{f}_0 + (\boldsymbol{f}_0\cdot \boldsymbol{s})\boldsymbol{s}) \big[\ln(4\sigma_0(1-\sigma_0)) - \ln\left(a^2+\delta^2\right) \big] - (\boldsymbol{f}_0 + (\boldsymbol{f}_0\cdot \boldsymbol{s})\boldsymbol{s}) + 2(\boldsymbol{f}_0 - (\boldsymbol{f}_0\cdot \boldsymbol{s})\boldsymbol{s}), \quad (20)$$

where $\boldsymbol{r}_0 = X(\sigma_0) - X(t)$. This is the regularized Keller–Rubinow formula.

4.4. ***The limit $\delta \to 0$.*** The first integral in (20) can be evaluated even when $\delta = 0$ because its singular behavior has been explicitly extracted. It is easy to see that in the limit $\delta \to 0$, the expression in (20) converges to the one obtained in [16]:

$$8\pi\mu \boldsymbol{v}(\sigma_0) = \int_{-\sigma_0}^{1-\sigma_0} \frac{\boldsymbol{f}(\sigma_0+t)}{r_0} + \frac{(\boldsymbol{f}(\sigma_0+t)\cdot \boldsymbol{r}_0)\boldsymbol{r}_0}{r_0^3} - \frac{\boldsymbol{f}_0 + (\boldsymbol{f}_0\cdot \boldsymbol{s})\boldsymbol{s}}{|t|}\, dt + (\boldsymbol{f}_0 + (\boldsymbol{f}_0\cdot \boldsymbol{s})\boldsymbol{s}) \big[\ln(4\sigma_0(1-\sigma_0)) - \ln a^2 \big] - (\boldsymbol{f}_0 + (\boldsymbol{f}_0\cdot \boldsymbol{s})\boldsymbol{s}) + 2(\boldsymbol{f}_0 - (\boldsymbol{f}_0\cdot \boldsymbol{s})\boldsymbol{s}).$$

4.5. ***Simplifications for $\delta > 0$.*** We note that since none of the functions in (20) is singular, one can evaluate the third term of the integral explicitly and include the result as part of the local terms, leaving only the integral of the stokeslet kernel as in the case of Lighthill's theory, (13). This also provides a way of comparing the two theories directly. The result is

$$8\pi\mu \boldsymbol{v}(\sigma_0) = 2\boldsymbol{f}_n - (\boldsymbol{f}_n + 2\boldsymbol{f}_\tau)\,[2\ln(\beta/\delta) + 1] + \int_{-\sigma_0}^{1-\sigma_0} \frac{\boldsymbol{f}(\sigma_0+t)}{\sqrt{r_0^2+\delta^2}} + \frac{(\boldsymbol{f}(\sigma_0+t)\cdot \boldsymbol{r}_0)\boldsymbol{r}_0}{r_0^2\sqrt{r_0^2+\delta^2}} dt. \quad (21)$$

This expression, found by the method of matched asymptotics, can be compared with (13), which was found by different means. The differences appear only in the local terms. We note that this final expression does not rely on the cancellation of singular terms.

In computations, although (21) does not contain singularities, the function is nearly singular (or spiky) so that there is a computational advantage to using (20) instead of (21).

4.6. ***The velocity of the fluid.*** The velocity field at an arbitrary point $\boldsymbol{x}$ in the fluid can also be evaluated using the asymptotic matching. The fluid velocity is given by the sum of the inner solution, (16), and the outer solution, (14), minus the inner expansion of the outer solution, given by the left-hand side of (18). After some cancellation, the final expression is

$$8\pi\mu\boldsymbol{u}(\boldsymbol{x}) = \int_0^1 \boldsymbol{f}(t)\,\frac{H_1(r)}{r} + (\boldsymbol{f}(t)\cdot\boldsymbol{r})\boldsymbol{r}\,\frac{H_2(r)}{r^3}\,dt \tag{22}$$
$$+\boldsymbol{f}(s)\left[1-\frac{(|\boldsymbol{x}_0|^2-\delta^2)(|\boldsymbol{x}_0|^2-a^2)}{(|\boldsymbol{x}_0|^2+\delta^2)^2}\right]-(\boldsymbol{f}\cdot\boldsymbol{s})\boldsymbol{s}\,\frac{a^2+\delta^2}{|\boldsymbol{x}_0|^2+\delta^2}-2(\boldsymbol{f}\cdot\boldsymbol{x}_0)\boldsymbol{x}_0\frac{a^2+\delta^2}{(|\boldsymbol{x}_0|^2+\delta^2)^2},$$

where $\boldsymbol{r}=\boldsymbol{x}-X(s+t)$, $r=|\boldsymbol{r}|$, and $\boldsymbol{x}_0=\boldsymbol{x}-X(s)$. Here $X(s)$ is the filament point closest to $\boldsymbol{x}$.

4.7. ***Periodic filaments.*** Equation (20) is valid for points along the filament that are far from the endpoints $s=0$ and $s=1$ relative to δ. In the case of a periodic filament, the choice of parametrization should be irrelevant. Therefore the equation can be evaluated at a valid point, say $s=1/2$, and the result should be valid for any point on the filament. The forces $\boldsymbol{f}(t)$ and parametrization $X(t)$ are periodic functions but one last modification is necessary because the function $1/\sqrt{t^2+\delta^2}$, which appears in the integrand of (20), is not periodic in t. In order to replace it with a periodic function, we use the identity

$$\int_{-1/2}^{1/2}\frac{1}{\sqrt{t^2+\delta^2}}\,dt=\int_{-1/2}^{1/2}\frac{dt}{\sqrt{(1/\pi^2)\sin^2(\pi t)+\delta^2}}-\ln(16/\pi^2)+O(\delta^2\ln\delta).$$

So, for a periodic filament, the final expression is

$$8\pi\mu\boldsymbol{v}(s)=\int_{-1/2}^{1/2}\frac{\boldsymbol{f}(s+t)}{(|\boldsymbol{r}_0|^2+\delta^2)^{1/2}}+\frac{(\boldsymbol{f}(s+t)\cdot\boldsymbol{r}_0)\boldsymbol{r}_0}{|\boldsymbol{r}_0|^2\,(|\boldsymbol{r}_0|^2+\delta^2)^{1/2}}-\frac{[\boldsymbol{f}(s)+(\boldsymbol{f}\cdot\boldsymbol{s})\boldsymbol{s}]}{\sqrt{\pi^{-2}\sin^2(\pi t)+\delta^2}}\,dt$$
$$+2(\boldsymbol{f}-(\boldsymbol{f}\cdot\boldsymbol{s})\boldsymbol{s})-(\boldsymbol{f}+(\boldsymbol{f}\cdot\boldsymbol{s})\boldsymbol{s})\left[\ln\frac{(a^2+\delta^2)\pi^2}{16}+1\right]. \tag{23}$$

We use this formulation, rather than (20), for periodic filaments.

We note that in this case, the local terms (outside the integral in (23)) can also be written as

$$2(\boldsymbol{f}-(\boldsymbol{f}\cdot\boldsymbol{s})\boldsymbol{s})-(\boldsymbol{f}+(\boldsymbol{f}\cdot\boldsymbol{s})\boldsymbol{s})\left[\ln(a^2)+1+\ln\frac{\pi^2(a^2+\delta^2)}{16a^2}\right].$$

It is clear that the choice of δ affects significantly the local drag. This is to be expected, since the regularization mostly affects the near-field velocity. However, it turns out that the local terms are exactly equal to the ones in [16], i.e.,

$$2(\boldsymbol{f} - (\boldsymbol{f}\cdot\boldsymbol{s})\boldsymbol{s}) - (\boldsymbol{f} + (\boldsymbol{f}\cdot\boldsymbol{s})\boldsymbol{s})(\ln a^2 + 1),$$

if δ is chosen so that $\ln \dfrac{\pi^2(a^2+\delta^2)}{16a^2} = 0$, or approximately $\delta = 0.788124a$.

5. Numerical examples

5.1. ***Validation studies.*** We consider first two validation studies by computing the velocity of the fluid around a translating slender body. The first test problem is that of a torus with centerline radius $R = 1/2\pi$ and cross-sectional radius a. The torus is slender when $\epsilon = a/R = 2\pi a \ll 1$. We consider here a torus translating in an arbitrary direction. The second validation study is that of a straight slender body of length 1 and radius a.

5.1.1. *A slender torus.* Consider a torus whose centerline is in the xy-plane. This is a particularly good test problem since the geometry of the slender body is that of a cylindrical tube with constant cross-section, which is exactly what our formulas have assumed. There is no exact solution; however, by placing various fundamental solutions along the centerline, Johnson and Wu [14] developed $O(\epsilon^2 \log \epsilon)$ asymptotic approximations to fluid velocities under various conditions. They give asymptotic formulas for the force per unit length on the centerline of the torus that produces a given translation. We make two comparisons. First, we compute forces by setting the centerline velocity to the prescribed value and using either (13) for Lighthill or (21) for Keller–Rubinow to solve for the forces. We also compute the centerline velocity when using the forces from [14] in the regularized theories. Second, we compute the fluid velocity using the regularized Keller–Rubinow formula (22) and compare with the results from [14].

In the first comparison, we set the centerline velocity to a constant and invert a trapezoid rule discretization of (13) to solve for the forces in Lighthill's theory. We do the same with (21) to solve for the forces in Keller–Rubinow's theory. The force per unit length is then compared with its asymptotic value given in [14]. The results for a horizontal translation velocity $(0, 1, 0)$ are shown in Table 1 and for a vertical translation velocity $(0, 0, 1)$ in Table 2. Recall that δ is a numerical parameter for the regularization of the integrals, and therefore should be related to the discretization size of the centerline. In these examples we discretize the centerline with N points in such a way that the point separation is approximately equal to the tube cross-section a; then δ is chosen proportional to $1/N$. The tables show results for two different values of δ for each slenderness value. The tables show that both theories give comparable results for the normal component of the

a	F_n^{JW}	F_n^{KR}	F_n^L	F_t^{JW}	F_t^{KR}	F_t^L	numerical parameters
0.01	2.2370	2.2539	2.2814	1.4213	1.4415	1.3822	$N = 100, \delta = 0.5/N$
		2.2177	2.2351		1.4008	1.3624	$N = 100, \delta = 0.4/N$
0.005	2.0149	2.0300	2.0453	1.2058	1.2191	1.1808	$N = 200, \delta = 0.5/N$
		1.9982	2.0080		1.1916	1.1665	$N = 200, \delta = 0.4/N$
0.0025	1.8245	1.8373	1.8468	1.0533	1.0630	1.0360	$N = 400, \delta = 0.5/N$
		1.8104	1.8166		1.0428	1.0249	$N = 400, \delta = 0.4/N$
0.00125	1.6636	1.6745	1.6809	0.93775	0.94528	0.92500	$N = 800, \delta = 0.5/N$
		1.6517	1.6559		0.92956	0.91605	$N = 800, \delta = 0.4/N$

Table 1. Comparison of the resultant force per unit length for the case of a torus of centerline radius $R = 1/2\pi$ and cross-sectional radius a translating horizontally (in the y-direction) with unit speed. The slenderness parameter defined in [14] is $\epsilon = 2\pi a$. The forces shown are for the normal and tangential components (subscripts) from [14] (JW), regularized Keller–Rubinow (KR), and regularized Lighthill (L). The number of points N discretizing the centerline is varied so that the point separation equals a. The Lighthill forces were found by inverting (13) while the Keller–Rubinow forces were found by inverting (21).

force. The Keller–Rubinow theory gives slightly better results for the tangential force and the given discretization parameters. By comparing (13) and (21), one can see that the dependence of the normal component of force on the velocity is identical for both theories, while there is a difference in the tangential component

a	F_n^{JW}	F_n^{KR}	F_n^L	numerical parameters
0.01	2.3503	2.3729	2.3729	$N = 100, \delta = 0.5/N$
		2.3259	2.3259	$N = 100, \delta = 0.4/N$
0.005	2.0806	2.0982	2.0982	$N = 200, \delta = 0.5/N$
		2.0614	2.0614	$N = 200, \delta = 0.4/N$
0.0025	1.8664	1.8805	1.8805	$N = 400, \delta = 0.5/N$
		1.8509	1.8509	$N = 400, \delta = 0.4/N$
0.00125	1.6922	1.7038	1.7038	$N = 800, \delta = 0.5/N$
		1.6795	1.6795	$N = 800, \delta = 0.4/N$

Table 2. Comparison of the resultant force per unit length for the case of a torus of centerline radius $R = 1/2\pi$ and cross-sectional radius a translating vertically (in the z-direction) with unit speed. The slenderness parameter defined in [14] is $\epsilon = 2\pi a$. The forces shown are for normal to the tube in the z-direction from [14] (JW), regularized Keller–Rubinow (KR), and regularized Lighthill (L). The number of points N discretizing the centerline is varied so that the point separation equals a. The Lighthill forces were found by inverting (13) while the Keller–Rubinow forces were found by inverting (21). Notice that these two equations are identical for the normal component of force since they only differ in the tangential force component. This example has zero tangential force so the two theories give the same answers.

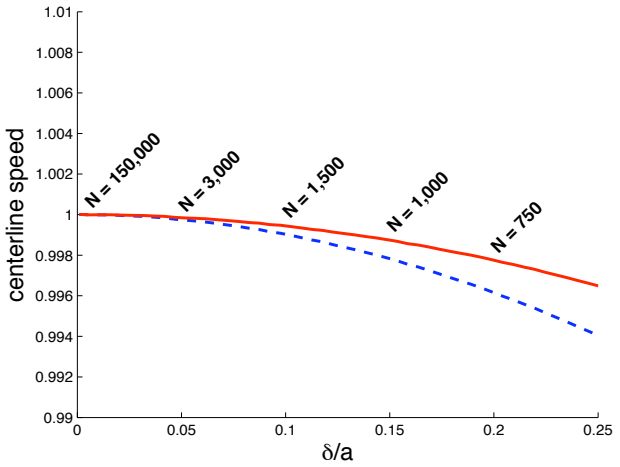

Figure 4. Centerline velocity of the torus as a function of δ when the force per unit length applied is the one given in [14] for a torus moving horizontally with constant velocity $(u, v, w) = (0, 1, 0)$. The solid curve corresponds to the Lighthill theory and the dashed curve to the Keller–Rubinow theory. N is the number of quadrature points along the centerline that were required to numerically resolve the integrals for the given value of δ.

of force. The test problem in Table 2 results in strictly normal force, which is why both theories give the same solution.

A different comparison was performed by using the values of the force per unit length given in [14] and applying those forces in the regularized theories. Although one expects the forces from each theory to be similar for a given centerline velocity boundary condition, they are not identical. So, using the asymptotic forces from [14] in the regularized theories does not guarantee the correct centerline velocity. We set $a = 0.01$ and use the asymptotic forces to compute the centerline velocities from (12) and (21) for different values of δ. The results for the torus translating horizontally in the y direction are shown in Figure 4. The solid curve corresponds to the Lighthill theory and the dashed curve to the Keller–Rubinow theory. For $a = 0.01$, the asymptotic error in [14] is $O(\epsilon^2 \log \epsilon) \approx 0.011$ where $\epsilon = 2\pi a$, which indicates that the velocity values are acceptable for $\delta \in (0, a/4]$. The figure also shows the number N of quadrature points on the centerline required to resolve the integrals for each δ. Note that N can be extremely large for $\delta \approx 0$; however, if we use, say, the value $\delta = 0.25a$, we can benefit tremendously by reducing the number of quadrature points due to the regularization of the integrands.

Finally, we compute the velocity in the fluid using the Keller–Rubinow theory, (22), and compare it to the asymptotic formula given in [14]. Figure 5 shows the y-component of the fluid velocity along the line $(x, 0, 0)$ where x varies form the surface of the torus to a distance of about $10a$. The left panel shows the result for $a = 0.01$, a value that allows the computation of the integrals with $N = 200$ points

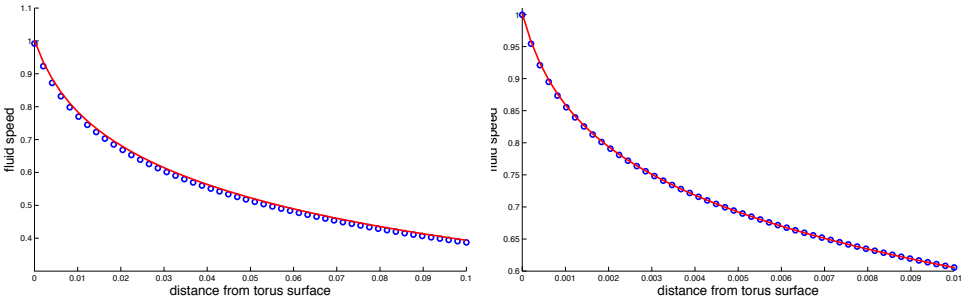

Figure 5. Fluid velocities resulting from tori moving horizontally with constant velocity $(u, v, w) = (0, 1, 0)$. The tori are given by centerline radius $R = 1/2\pi$ and cross-sectional radius $a = 0.01$ (left) and $a = 0.001$ (right). The plots show the y component of velocity v at points $(x, 0, 0)$ as x varies from the torus surface to $x = 10a$. The velocities for the Johnson and Wu theory [14] are shown as circles. The solid line represents the velocities for the regularized Keller–Rubinow theory with $\delta = 0.4/N$ and $N = 200$ (left) and $N = 2000$ (right).

on the centerline. The right panel shows the results for $a = 0.001$ and $N = 2000$. In this case, the forces used in the Keller–Rubinow theory were computed by inverting (21) by enforcing the velocity boundary condition on a curve on the outer surface of the torus (the curve corresponding to $r = R + a$, $z = 0$). The circles represent the asymptotic theory in [14] while the solid line is from Keller–Rubinow. Note that the agreement is better for the more slender torus.

5.1.2. *A straight slender body.* The second validation problem is the one of a straight slender filament of unit length. Chwang and Wu [4] developed an exact solution for the translation of a prolate spheroid, which we use as a reference. We emphasize that our formulas have been derived for a cylindrical tube of constant circular cross-section, as depicted in Figure 6, so the geometry is not exactly the same as the solution in [4]. For this reason, we cannot expect our solution to converge to the one in [4]; however, a qualitative comparison is instructive. For the regularized theories, we use a slender cylinder whose axis coincides with the x-axis and whose radius is $a = 0.01$. The reference is the exact solution for the prolate spheroid $4x^2 + (y^2 + z^2)/a^2 = 1$. The two slender bodies have the same cross section when $x = 0$ only as shown in Figure 6. At other values of x, the cylinder is wider than the prolate spheroid. We invert a discrete version of (22) based on the trapezoid rule with $N = 401$ points, enforcing the velocity boundary condition of $(u, v, w) = (1, 1, 0)$ on the surface of the cylinder ($y = a$).

We then select points in the fluid along a straight line perpendicular to the slender bodies and emanating from the center of them, given by $(0, y, 0)$ for $y \in [a, 10a]$ (see Figure 6 for reference). We compute the fluid velocity there using both the regularized Keller–Rubinow theory for the cylindrical tube and the exact solution of Chwang and Wu for the prolate spheroid. The results are shown on the left panel of

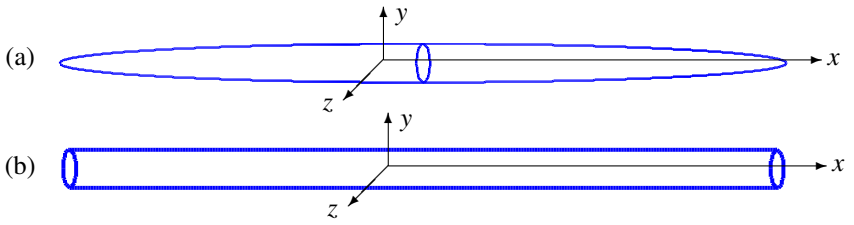

Figure 6. Difference in the shape of slender bodies. Panel (a) shows the prolate spheroid for which an exact solution is known [4]. Panel (b) shows the shape addressed in our work. The figures use a radius of $a = 0.025$ for visualization purposes. The cross-sections are equal only at $x = 0$.

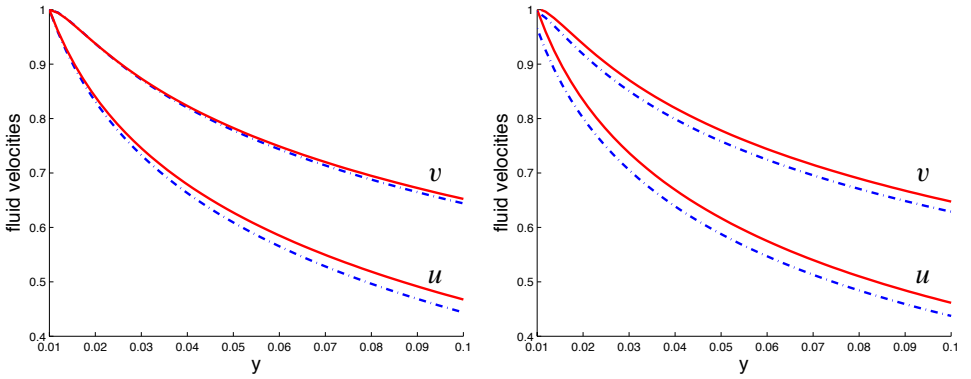

Figure 7. Fluid velocities resulting from a straight slender body moving with constant velocity $(u, v, w) = (1, 1, 0)$. The axis of the slender body is the x axis. The length of the body is 1 and the radius is $a = 0.01$. The number of quadrature points was $N = 401$ and $\delta = 0.5/N$. The left panel shows the x and the y components of velocity (u, v) at points $(0, y, 0)$ for $y \in [a, 10a]$. The right panel shows the same velocity components at points $(0.25, y, 0)$, at a cross section halfway between the center and the nose of the tube. The solid curves are from the regularized Keller–Rubinow theory while the dashed lines are the exact solution of a prolate spheroid given in [4].

Figure 7. The solid curves are for the straight cylinder using the regularized Keller–Rubinow theory and the dashed curves are the exact prolate spheroid solution. The right panel of the figure shows similar results but computing the fluid velocity along the line $(0.25, y, 0)$ for $a \le y \le 10a$, which is halfway between the center and the nose of the slender bodies. Here we do not expect the solutions to agree due to the fact that the two slender bodies are different. Specifically, the velocities given by Chwang and Wu are not equal to 1 at the point $(0.25, a, 0)$ since that is not on the surface of the prolate spheroid, but it is on the surface of the slender cylinder. In spite of this, the curves agree qualitatively.

5.2. ***Application: Closed filaments.*** We apply both theories to the problem of closed filaments with a normal force proportional to curvature. Our filaments are

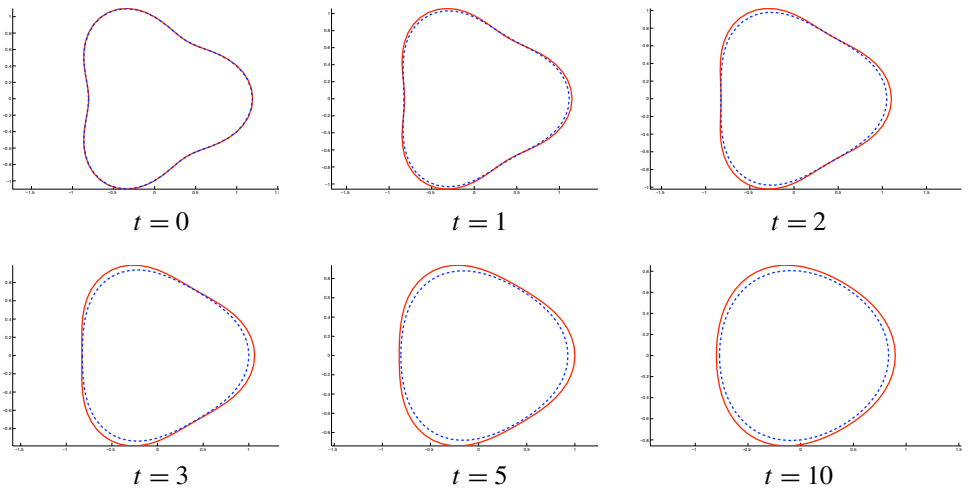

Figure 8. A closed filament $r = 1 + B\cos(n\theta)$ with normal forces at various times with $B = 0.2$, $N = 64$, $n = 3$. The slender body radius was $a = 0.1$ and the regularization parameter set to $\delta = 0.1$. The dashed lines correspond to Lighthill's theory, and the solid lines are results for the Keller–Rubinow method.

defined in cylindrical coordinates by

$$r = 1 + B\cos(n\theta) \quad \text{and} \quad z = 0$$

for various integers n, and we assign a force

$$F(\theta, t) = -\frac{1}{10}\kappa(\theta, t)\nu(\theta, t)\left(L(t) - \frac{3\pi}{2}\right)$$

where $\kappa(\theta, t)$ is the curvature of the filament, $\nu(\theta, t)$ is the inward unit normal, and $L(t)$ is the arclength of the filament. We expect such forces to restore the filaments to circular shapes. The filaments are discretized using N points and the forces are computed at those locations. Since the filaments and forces are smooth and periodic, we approximate derivatives along the filament using FFT interpolation and evaluate the integrals with a trapezoid rule. We update positions at each time step with a Runge-Kutta method. Results for both the Lighthill and Keller–Rubinow theories, (13) and (23) respectively, can be seen in Figure 8 for $r = 1 + B\cos(n\theta)$ with $B = 0.2$, $N = 64$, $n = 3$. The slender body radius was $a = 0.1$ and the regularization parameter set to $\delta = 0.1$. The differences in the shapes are due to the local terms in the expressions since the integrals are identical. The figure shows that for this set of parameters, the filament approaches the circular shape faster with Lighthill's method.

It has been noted in the Introduction that subtracting the singularity of the Keller–Rubinow integral like in (20) or (23) can lead to numerical instabilities in filaments with high frequency components. This is the case when the parameter δ is chosen

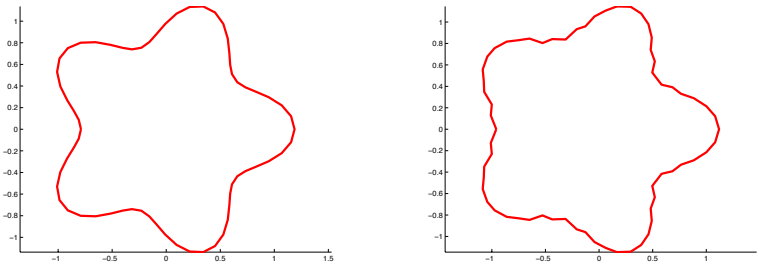

Figure 9. Solution at time $t = 1$ using the regularized theory of Keller–Rubinow, (21). The closed filament was given initially by $r = 1 + B\cos(n\theta)$ with $B = 0.3$, $N = 64$, $n = 5$. The slender body radius was $a = 0.1$ and two different regularizations were used. Note the formation of instabilities in the filament with less regularization.

too small for the regularization to provide stability. Figure 9 shows a closed filament with wave number $n = 5$ after a short simulation time using two different values of the regularization parameter δ. The smaller value is too small to prevent instabilities. Figure 10 shows that the filament computation remains stable for long times when the larger regularization parameter is used. The computations were done using (23).

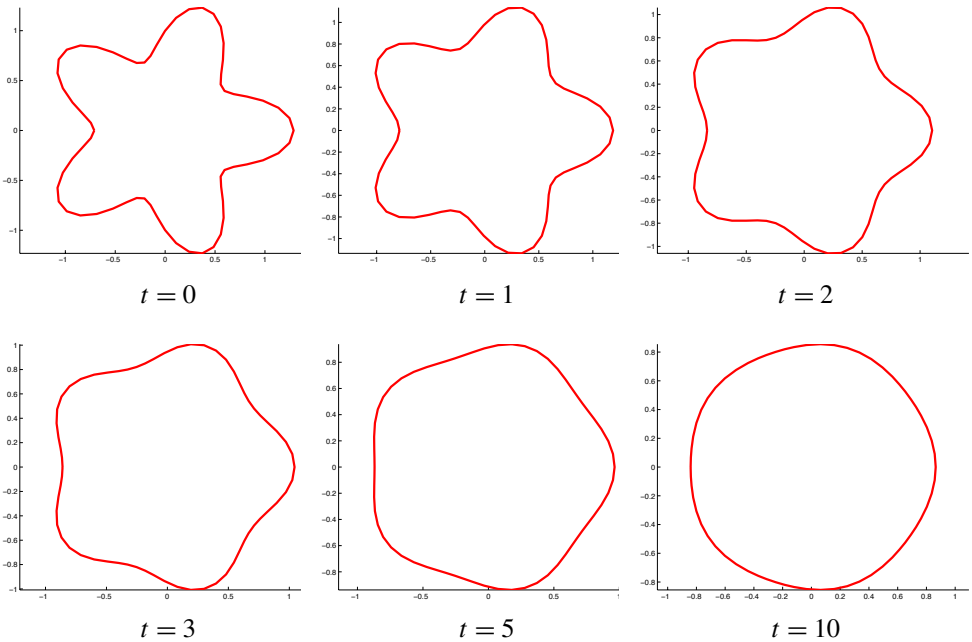

Figure 10. Solution at various times using the regularized theory of Keller and Rubinow, (21). The closed filament was given initially by $r = 1 + B\cos(n\theta)$ with $B = 0.3$, $N = 64$, $n = 5$. The slender body radius was $a = 0.1$ and the regularization parameter set to $\delta = 0.1$.

5.3. ***Application: Swimming organism.*** Biological applications of slender body theory also call for open filaments such as in the case of cilia or flagella. Sperm swimming in an infinite fluid, for example, often exhibit planar beat in which a wave travels along the flagellum from head to tail. Internal mechanisms in the flagellum produce time-dependent forces along it that result in swimming motions through interactions with the fluid. Relevant mathematical analysis and computational modeling of swimming "filaments" or cylindrical tubes can be found in [10; 23; 3; 4; 14; 6]. Our goal is to show the applicability of our result to this type of motion, so we present an idealized swimming microorganism modeled as a single sinusoidal filament with growing amplitude from head to tail. Simulations of the motion and flow field around flagella in which the shape was represented parametrically are found, for example, in [7; 9; 22; 21].

In time, the organism moves according to a traveling wave translating down the body. There are two types of forces involved. The organism is defined by N points equally distributed along the length which lies in the xy-plane so that the organism points are $(x_k, y_k, 0)$ for $k = 1, 2, \ldots, N$. Consecutive points are connected by springs whose resting lengths are given by their initial position. The first type of force is the spring force (Hooke's law) that develops as the end points of the springs move causing them to contract or stretch. The second type of force is due to an imposed time-dependent curvature of the filament consistent with the idealized shape

$$y(x) = Y_0\, x\ \sin\left(\frac{2\pi}{L}(x-t)\right), \qquad 0 \le x \le L.$$

This is done by writing a discrete energy function

$$\mathscr{E}_h(x_1, y_1, \ldots, x_k, y_k, \ldots, x_N, y_N) = \frac{h}{2} S_1 \sum_{n=1}^{N} \left(\frac{(\vec{x}_{n+1} - \vec{x}_n) \times (\vec{x}_n - \vec{x}_{n-1})}{h^3} - \kappa_n \right)^2$$

where h is the separation between contiguous points, S_1 is a constant and κ_n is the target curvature at point n. The cross product is known to approximate curvature [9]. Then the curvature force is defined as

$$\vec{F}_k = -\left(\frac{\partial \mathscr{E}_h}{\partial x_k}, \frac{\partial \mathscr{E}_h}{\partial y_k}, 0 \right).$$

By defining forces this way, we guarantee that the net force and net torque are identically zero. More details of this force can be found in [9; 8; 5]. The goal of this example is show an application of the methodology developed here even if the biological aspects are not developed.

The flagellum is defined by N points equally distributed along the length. Their velocities are computed using the trapezoid rule on the Keller–Rubinow integral in (21), and the position is updated at each time step with Euler's method. The

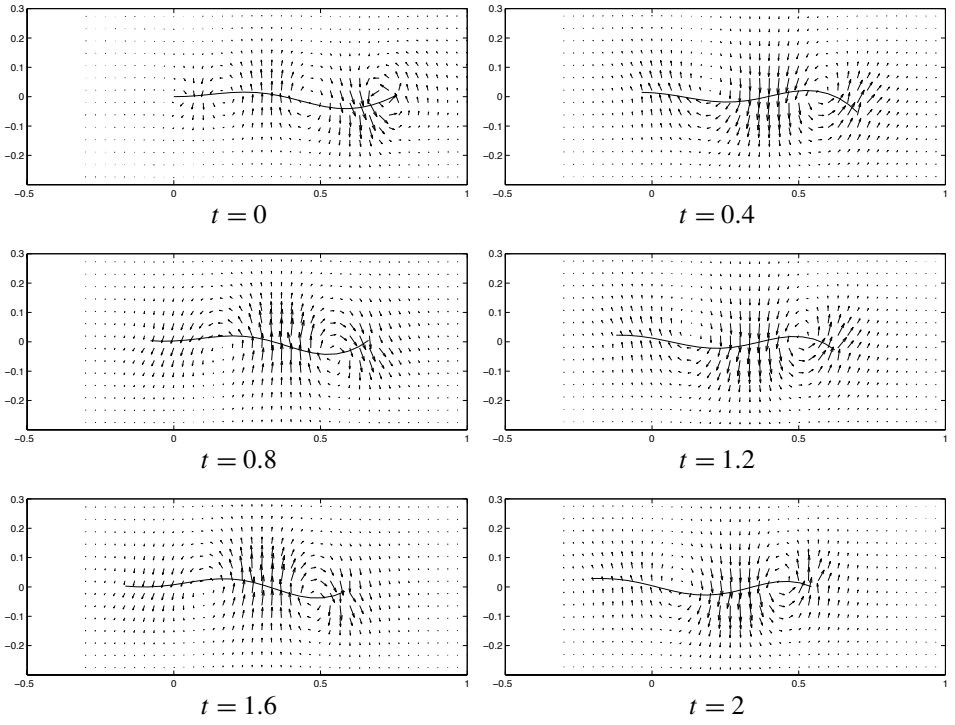

Figure 11. Snapshots of the flagella at different times. The motion is governed by (21), and the fluid velocities are calculated using (22). For these calculations, the length of the flagella is $L = 0.75$, and we have used $N = 20$ nodes with $\delta = 2h = 2L/(N-1)$ and $a = 2\delta$.

fluid velocities are computed using the trapezoid rule on the integral in (22). All necessary derivatives along the filament are calculated with simple finite differences. Figure 11 shows the results for the parameters $L = 0.75$, $N = 20$, $\delta = 2h = 2L/(N-1)$ and $a = 2\delta$. This results in a dimensionless oscillation period of $T = 0.75$ so that the snapshots in the figure cover more than two periods. The time step was set to $\Delta t = 10^{-5}$. All frames cover exactly the same spatial domain so that the swimming motion (leftward) of the organism is appreciable. The fluid motion in the plane of the organism shows the rotations that are typical of this motion [9; 8; 5].

6. Conclusions

We have derived a regularized formulation of the slender body theories developed by Lighthill and by Keller and Rubinow. The main purpose is to provide a modified version of each theory that retains the asymptotic order of the original formula but results in expressions that are more amenable to computation. Specifically, the

Keller and Rubinow theory relies on the exact cancellation of singular functions, which is not possible to accomplish numerically without some type of regularization. In the case of Lighthill's theory, the advantage of our approach is that the gap that is removed from the line integral can be restored. The uninterrupted integral along the centerline of the slender body is important especially in closed filaments where one can take advantage of the periodicity of the problem using high-order quadratures.

The results show that both regularized theories result in the same integral along the filament, (13) and (21), which allows a direct comparison between them. The two theories differ by the local terms only due to the way in which they are derived and the order of the asymptotic expansions. The regularization parameter δ should be considered a numerical parameter that removes the singularity of the original expressions in a way that maintains the asymptotic order and stabilizes the computation of the integrals. The validation studies show that comparable results can be obtained with $\delta \approx 0$ and $\delta = O(a)$ while the latter case provides a substantial advantage in the number of quadrature points needed to compute the resulting integrals accurately. We show by example that sufficient regularization (i.e. large enough δ) is necessary to stabilize high wave numbers in the representation of the filaments.

The theory presented here involves regularized stokeslets and dipoles along the centerline of the slender body. The inclusion of other elements, such as rotlets for a torque load, is also possible since regularized versions of them are available [1].

Appendix A: Details of the inner velocity expansion

To compute the inner velocity in (15), we will need the following approximations for $|\boldsymbol{x}_0| = \rho \ll q$:

$$J_1 = \int_{-q}^{q} \frac{H_1(\sqrt{|\boldsymbol{x}_0|^2+z^2})\,dz}{(|\boldsymbol{x}_0|^2+z^2)^{1/2}} \approx \ln\frac{4q^2}{|\boldsymbol{x}_0|^2+\delta^2} + \frac{2\delta^2}{|\boldsymbol{x}_0|^2+\delta^2} + \frac{\left(|\boldsymbol{x}_0|^2-\delta^2\right)}{2q^2}$$

$$J_{2a} = \int_{-q}^{q} \frac{H_3(\sqrt{|\boldsymbol{x}_0|^2+z^2})\,dz}{(|\boldsymbol{x}_0|^2+z^2)^{3/2}} \approx \frac{2(|\boldsymbol{x}_0|^2-\delta^2)}{(|\boldsymbol{x}_0|^2+\delta^2)^2} - \frac{1}{q^2}$$

$$J_{2b} = \int_{-q}^{q} \frac{H_2(\sqrt{|\boldsymbol{x}_0|^2+z^2})\,dz}{(|\boldsymbol{x}_0|^2+z^2)^{3/2}} \approx \frac{2}{(|\boldsymbol{x}_0|^2+\delta^2)} - \frac{1}{q^2}$$

$$J_3 = \int_{-q}^{q} \frac{H_4(\sqrt{|\boldsymbol{x}_0|^2+z^2})\,dz}{(|\boldsymbol{x}_0|^2+z^2)^{5/2}} \approx \frac{4}{3(|\boldsymbol{x}_0|^2+\delta^2)^2} - \frac{1}{2q^4}$$

$$J_4 = \int_{-q}^{q} \frac{zH_2(\sqrt{|\boldsymbol{x}_0|^2+z^2})dz}{(|\boldsymbol{x}_0|^2+z^2)^{3/2}} = 0$$

$$J_5 = \int_{-q}^{q} \frac{z H_4(\sqrt{|\boldsymbol{x}_0|^2+z^2})dz}{(|\boldsymbol{x}_0|^2+z^2)^{5/2}} = 0$$

$$J_6 = \int_{-q}^{q} \frac{z^2 H_2(\sqrt{|\boldsymbol{x}_0|^2+z^2})\,dz}{(|\boldsymbol{x}_0|^2+z^2)^{3/2}} \approx \ln\frac{4q^2}{|\boldsymbol{x}_0|^2+\delta^2} - 2 + \frac{3(|\boldsymbol{x}_0|^2+\delta^2)}{2q^2}$$

$$J_7 = \int_{-q}^{q} \frac{z^2 H_4(\sqrt{|\boldsymbol{x}_0|^2+z^2})\,dz}{(|\boldsymbol{x}_0|^2+z^2)^{5/2}} \approx \frac{2}{3(|\boldsymbol{x}_0|^2+\delta^2)} - \frac{1}{q^2}$$

Neglecting terms of order $O(a^2/q^2)$, $O(\delta^2/q^2)$ and $O(|\boldsymbol{x}_0|^2/q^2)$, the velocity can be written as

$$\begin{aligned}
8\pi\mu(\boldsymbol{u}(\boldsymbol{x}_0)-\boldsymbol{U}) &= \boldsymbol{f}(J_1-2AJ_{2a})+(\boldsymbol{f}\cdot\boldsymbol{x}_0)\boldsymbol{x}_0\,(J_{2b}+6AJ_3)+(\boldsymbol{f}\cdot\boldsymbol{s})\boldsymbol{s}\,(J_6+6AJ_7)\\
&= \boldsymbol{f}\left[\ln\frac{4q^2}{|\boldsymbol{x}_0|^2+\delta^2}+\frac{2\delta^2}{|\boldsymbol{x}_0|^2+\delta^2}-2A\left(\frac{2|\boldsymbol{x}_0|^2-\delta^2}{(|\boldsymbol{x}_0|^2+\delta^2)^2}-\frac{1}{q^2}\right)\right]\\
&\quad+(\boldsymbol{f}\cdot\boldsymbol{x}_0)\boldsymbol{x}_0\left[\frac{2}{|\boldsymbol{x}_0|^2+\delta^2}+6A\left(\frac{4}{3(|\boldsymbol{x}_0|^2+\delta^2)^2}\right)\right]\\
&\quad+(\boldsymbol{f}\cdot\boldsymbol{s})\boldsymbol{s}\left[\ln\frac{4q^2}{|\boldsymbol{x}_0|^2+\delta^2}-2+6A\left(\frac{2}{3(|\boldsymbol{x}_0|^2+\delta^2)}-\frac{1}{q^2}\right)\right].
\end{aligned}$$

When the evaluation point is on the surface, $|\boldsymbol{x}_0| = a$, the velocity must be independent of the particular surface point, so that the coefficient of $(\boldsymbol{f}\cdot\boldsymbol{x}_0)\boldsymbol{x}_0$ must vanish. This leads to

$$A = -\frac{a^2+\delta^2}{4},$$

so that this choice of A is consistent with the boundary conditions at the filament surface, we have for $|\boldsymbol{x}_0| = a$

$$8\pi\mu\boldsymbol{U} = 8\pi\mu\boldsymbol{v}(s) - (\boldsymbol{f}+(\boldsymbol{f}\cdot\boldsymbol{s})\boldsymbol{s})\left[\ln\frac{4q^2}{a^2+\delta^2}+1\right]+4(\boldsymbol{f}\cdot\boldsymbol{s})\boldsymbol{s},$$

and the final velocity expression is (16):

$$\begin{aligned}
8\pi\mu\boldsymbol{u}(\boldsymbol{x}_0) = 8\pi\mu\boldsymbol{v}(\sigma_0) &- (\boldsymbol{f}_0+(\boldsymbol{f}_0\cdot\boldsymbol{s})\boldsymbol{s})\left[\ln\frac{|\boldsymbol{x}_0|^2+\delta^2}{a^2+\delta^2}+\frac{(|\boldsymbol{x}_0|^2-\delta^2)(|\boldsymbol{x}_0|^2-a^2)}{(|\boldsymbol{x}_0|^2+\delta^2)^2}\right]\\
&+2(\boldsymbol{f}_0\cdot\boldsymbol{s})\boldsymbol{s}\frac{|\boldsymbol{x}_0|^2(|\boldsymbol{x}_0|^2-a^2)}{(|\boldsymbol{x}_0|^2+\delta^2)^2}+2(\boldsymbol{f}_0\cdot\boldsymbol{x}_0)\boldsymbol{x}_0\frac{|\boldsymbol{x}_0|^2-a^2}{(|\boldsymbol{x}_0|^2+\delta^2)^2}+O(\epsilon^2),
\end{aligned}$$

where

$$\epsilon = \max\Big(\frac{|\boldsymbol{x}_0|}{q},\frac{\delta}{q}\Big).$$

Appendix B: Matching

Consider the matching equation

$$\int_0^1 J(\boldsymbol{r},\rho,\delta,\boldsymbol{f}(\sigma))\,d\sigma = 8\pi\mu\boldsymbol{v}(s) - (\boldsymbol{f}+(\boldsymbol{f}\cdot\boldsymbol{s})\boldsymbol{s})\left[\ln\frac{\rho^2+\delta^2}{a^2+\delta^2}+1\right]+2(\boldsymbol{f}\cdot\boldsymbol{s})\boldsymbol{s}+\frac{2(\boldsymbol{f}\cdot\boldsymbol{x}_0)\boldsymbol{x}_0}{\rho^2}. \quad (24)$$

Since the terms containing ρ came from integrals J_1, J_{2b} and J_6, it is natural to consider writing

$$\begin{aligned}\int_0^1 J(\boldsymbol{r},\rho,\delta,\boldsymbol{f}(\sigma))\,d\sigma &= \int_0^1 \big(J(\boldsymbol{r},\rho,\delta,\boldsymbol{f}(\sigma))-\boldsymbol{f}(s)K_1(\rho,\delta)-(\boldsymbol{f}\cdot\boldsymbol{x}_0)\boldsymbol{x}_0K_2(\rho,\delta)-(\boldsymbol{f}\cdot\boldsymbol{s})\boldsymbol{s}K_3(\rho,\delta)\big)\,d\sigma\\ &\quad+\int_0^1 [\boldsymbol{f}(s)K_1(\rho,\delta)+(\boldsymbol{f}\cdot\boldsymbol{x}_0)\boldsymbol{x}_0K_2(\rho,\delta)+(\boldsymbol{f}\cdot\boldsymbol{s})\boldsymbol{s}K_3(\rho,\delta)]d\sigma, \quad (25)\end{aligned}$$

where, setting $t=\sigma-s$, we define

$$K_1(\rho,\delta)=\frac{H_1(\sqrt{t^2+\rho^2})}{(t^2+\rho^2)^{1/2}},\qquad K_2(\rho,\delta)=\frac{H_2(\sqrt{t^2+\rho^2})}{(t^2+\rho^2)^{3/2}},$$
$$K_3(\rho,\delta)=\frac{H_2(\sqrt{t^2+\rho^2})\,t^2}{(t^2+\rho^2)^{3/2}}.$$

We approximate the first integral on the right-hand side of (25) by setting $\rho=0$ so that the outer solution is approximated by

$$\begin{aligned}\int_0^1 J(\boldsymbol{r},\rho,\delta,\boldsymbol{f}(\sigma))\,d\sigma &\approx \int_0^1 [J(\boldsymbol{r}_0,0,\delta,\boldsymbol{f}(\sigma))-\boldsymbol{f}(s)K_1(0,\delta)-(\boldsymbol{f}\cdot\boldsymbol{s})\boldsymbol{s}K_3(0,\delta)]d\sigma\\ &\quad+\int_0^1 [\boldsymbol{f}(s)K_1(\rho,\delta)+(\boldsymbol{f}\cdot\boldsymbol{x}_0)\boldsymbol{x}_0K_2(\rho,\delta)+(\boldsymbol{f}\cdot\boldsymbol{s})\boldsymbol{s}K_3(\rho,\delta)]d\sigma, \quad (26)\end{aligned}$$

where $\boldsymbol{r}_0=X(s)-X(s+t)$.

Then, by using the integrals

$$\begin{aligned}\int_0^1 K_1(\rho,\delta)\,d\sigma &= \int_{-s}^{1-s}\frac{(t^2+\rho^2+2\delta^2)\,dt}{(t^2+\rho^2+\delta^2)^{3/2}}\\ &= \ln(4s(1-s))-\ln(\rho^2+\delta^2)+O(\rho^2)+O(\delta^2),\\ \int_0^1 K_2(\rho,\delta)\,d\sigma &= \int_{-s}^{1-s}\frac{dt}{(t^2+\rho^2+\delta^2)^{3/2}}\\ &= \frac{2}{\rho^2+\delta^2}+O(\rho^2)=\frac{2}{\rho^2}+O(\rho^2)+O(\delta^2/\rho^2),\end{aligned}$$

$$\int_0^1 K_3(\rho,\delta)\,d\sigma = \int_{-s}^{1-s} \frac{t^2\,dt}{(t^2+\rho^2+\delta^2)^{3/2}} = \ln(4s(1-s)) - 2 - \ln(\rho^2+\delta^2) + O(\rho^2),$$

(see the expressions in (7)), Equation (24) becomes

$$\begin{aligned}\int_0^1 \big(J(\boldsymbol{r}_0,0,\delta,\boldsymbol{f}(\sigma)) - \boldsymbol{f}_0 K_1(0,\delta) - (\boldsymbol{f}_0\cdot\boldsymbol{s})\boldsymbol{s}K_3(0,\delta)\big)\,d\sigma \\ + (\boldsymbol{f}_0 + (\boldsymbol{f}_0\cdot\boldsymbol{s})\boldsymbol{s})\big[\ln(4s(1-s)) - \ln(\rho^2+\delta^2)\big] - 2(\boldsymbol{f}_0\cdot\boldsymbol{s})\boldsymbol{s} + \frac{2(\boldsymbol{f}_0\cdot\boldsymbol{x}_0)\boldsymbol{x}_0}{\rho^2} \\ = 8\pi\mu\boldsymbol{v}(s) - (\boldsymbol{f}_0 + (\boldsymbol{f}_0\cdot\boldsymbol{s})\boldsymbol{s})\left[\ln\frac{\rho^2+\delta^2}{a^2+\delta^2} + 1\right] + 2(\boldsymbol{f}_0\cdot\boldsymbol{s})\boldsymbol{s} + \frac{2(\boldsymbol{f}_0\cdot\boldsymbol{x}_0)\boldsymbol{x}_0}{\rho^2}.\end{aligned}$$

Appendix C: Simplifying the velocity expression

The filament velocity formula (19) can be simplified by using (7) and the identity

$$\int_{-s}^{1-s} \frac{dt}{(t^2+a^2+\delta^2)^{1/2}} = \ln(4s(1-s)) - \ln\big(a^2+\delta^2\big) + O(a^2+\delta^2);$$

we can write the filament velocity as

$$\begin{aligned}8\pi\mu\boldsymbol{v}(s) = &\int_{-s}^{1-s} \frac{\boldsymbol{f}(s+t)}{(|\boldsymbol{r}_0|^2+\delta^2)^{1/2}} + \frac{(\boldsymbol{f}(s+t)\cdot\boldsymbol{r}_0)\boldsymbol{r}_0}{|\boldsymbol{r}_0|^2\,(|\boldsymbol{r}_0|^2+\delta^2)^{1/2}} - \frac{\boldsymbol{f}(s)+(\boldsymbol{f}\cdot\boldsymbol{s})\boldsymbol{s}}{(t^2+\delta^2)^{1/2}}\,dt \\ &+ \delta^2\int_{-s}^{1-s} \frac{\boldsymbol{f}(s+t)}{(|\boldsymbol{r}_0|^2+\delta^2)^{3/2}} - \frac{(\boldsymbol{f}(s+t)\cdot\boldsymbol{r}_0)\boldsymbol{r}_0}{|\boldsymbol{r}_0|^2\,(|\boldsymbol{r}_0|^2+\delta^2)^{3/2}} - \frac{\boldsymbol{f}(s)-(\boldsymbol{f}\cdot\boldsymbol{s})\boldsymbol{s}}{(t^2+\delta^2)^{3/2}}\,dt \\ &+ \int_{-s}^{1-s} \frac{\boldsymbol{f}(s)+(\boldsymbol{f}\cdot\boldsymbol{s})\boldsymbol{s}}{(t^2+a^2+\delta^2)^{1/2}}\,dt - (\boldsymbol{f}+(\boldsymbol{f}\cdot\boldsymbol{s})\boldsymbol{s}) + 2(\boldsymbol{f}-(\boldsymbol{f}\cdot\boldsymbol{s})\boldsymbol{s}),\end{aligned}$$

where $\boldsymbol{r}_0 = X(s) - X(s+t)$.

Lemma 6.1 below shows that the second integral in this expression is $O(\delta^2\ln\delta)$, so that the final expression for the filament velocity up to this order is

$$\begin{aligned}8\pi\mu\boldsymbol{v}(s) = &\int_{-s}^{1-s} \frac{\boldsymbol{f}(s+t)}{(|\boldsymbol{r}_0|^2+\delta^2)^{1/2}} + \frac{(\boldsymbol{f}(s+t)\cdot\boldsymbol{r}_0)\boldsymbol{r}_0}{|\boldsymbol{r}_0|^2\,(|\boldsymbol{r}_0|^2+\delta^2)^{1/2}} - \frac{\boldsymbol{f}(s)+(\boldsymbol{f}\cdot\boldsymbol{s})\boldsymbol{s}}{(t^2+\delta^2)^{1/2}}\,dt \\ &+ \int_{-s}^{1-s} \frac{\boldsymbol{f}(s)+(\boldsymbol{f}\cdot\boldsymbol{s})\boldsymbol{s}}{(t^2+a^2+\delta^2)^{1/2}}\,dt - (\boldsymbol{f}+(\boldsymbol{f}\cdot\boldsymbol{s})\boldsymbol{s}) + 2(\boldsymbol{f}-(\boldsymbol{f}\cdot\boldsymbol{s})\boldsymbol{s}).\end{aligned}$$

Lemma 6.1. *Let a filament be defined by the curve $X(t)$, where t is the arclength parameter. Let $f(t)$ be a smooth function, $\boldsymbol{r}(t) = X(t) - X(0)$ and $\delta \ll \ell$. Then*

$$I(\delta) = \delta^2\int_{-\ell}^{\ell} \frac{f(t)}{(|\boldsymbol{r}|^2+\delta^2)^{3/2}} - \frac{f(0)}{(t^2+\delta^2)^{3/2}}\,dt = -\big(\tfrac{1}{4}K_0^2 f_0 + f_0''\big)\delta^2\ln\delta + O(\delta^2)$$

where $f_0 = f(0)$, $f_0' = f'(0)$, $f_0'' = f''(0)$ and K_0 is the filament curvature at $X(0)$.

Proof. Consider first the integral

$$I_1(\delta) = \delta^2 \int_0^\ell \frac{f(t)}{(|\boldsymbol{r}(t)|^2 + \delta^2)^{3/2}}\, dt$$

and write for $t \ll 1$

$$\begin{aligned}
\boldsymbol{r}(t) &= t\hat{\tau} + \tfrac{1}{2}t^2 K_0 \hat{n} + \tfrac{1}{6}t^3 (K_0' \hat{n} - K_0^2 \hat{\tau}) + O(t^4),\\
|\boldsymbol{r}(t)|^2 &= \boldsymbol{r}\cdot\boldsymbol{r} = t^2 - \tfrac{1}{12}K_0^2 t^4 + O(t^5),\\
|\boldsymbol{r}(t)| &= t - \tfrac{1}{24}K_0^2 t^3 + O(t^4),\\
|\boldsymbol{r}(t)|_t &= 1 - \tfrac{1}{8}K_0^2 t^2 + O(t^3).
\end{aligned}$$

where $\hat{\tau}$ and $\hat{n}$ are the tangent and normal unit vectors at $X(0)$. Using these expressions we write for $t \ll 1$

$$\begin{aligned}
f(t) &= f_0 + t f_0' + \tfrac{1}{2}t^2 f_0'' + O(t^3)\\
&= f_0 |\boldsymbol{r}(t)|_t \left[1 + \tfrac{1}{8}K_0^2 |\boldsymbol{r}(t)|^2\right] + f_0' |\boldsymbol{r}(t)| |\boldsymbol{r}(t)|_t + \tfrac{1}{2} f_0'' |\boldsymbol{r}(t)|^2 |\boldsymbol{r}(t)|_t + O(t^3)\\
&= |\boldsymbol{r}(t)|_t \left[f_0 + |\boldsymbol{r}(t)| f_0' + \tfrac{1}{2}|\boldsymbol{r}(t)|^2 \left(f_0'' + \tfrac{1}{4}K_0^2 f_0\right)\right] + O(t^3)\\
&= |\boldsymbol{r}(t)|_t \, \mathcal{A}(|\boldsymbol{r}(t)|) + O(t^3).
\end{aligned}$$

Then

$$\begin{aligned}
I_1(\delta) &= \delta^2 \int_0^\ell \frac{f(t) - |\boldsymbol{r}(t)|_t \, \mathcal{A}(|\boldsymbol{r}(t)|)}{(|\boldsymbol{r}(t)|^2 + \delta^2)^{3/2}}\, dt + \delta^2 \int_0^\ell \frac{|\boldsymbol{r}(t)|_t \, \mathcal{A}(|\boldsymbol{r}(t)|)}{(|\boldsymbol{r}(t)|^2 + \delta^2)^{3/2}}\, dt\\
&= J_1(\delta) + J_2(\delta).
\end{aligned}$$

By construction we know that $J_1(\delta) = O(\delta^2)$. On the other hand, we can let $y = |\boldsymbol{r}(t)|$ and write

$$J_2(\delta) = \delta^2 \int_0^R \frac{\mathcal{A}(y)}{(y^2 + \delta^2)^{3/2}}\, dy$$

where $R = |\boldsymbol{r}(\ell)|$. So

$$\begin{aligned}
J_2(\delta) = f_0 \int_0^R \frac{\delta^2}{(y^2+\delta^2)^{3/2}}\, dy + f_0' \int_0^R \frac{\delta^2 y}{(y^2+\delta^2)^{3/2}}\, dy\\
+ \tfrac{1}{2}\left(f_0'' + \tfrac{1}{4}K_0^2 f_0\right) \int_0^R \frac{\delta^2 y^2}{(y^2+\delta^2)^{3/2}}\, dy
\end{aligned}$$

or

$$\begin{aligned}
J_2(\delta) = f_0 \frac{R}{\sqrt{R^2+\delta^2}} - f_0' \left[\frac{\delta^2}{\sqrt{R^2+\delta^2}} - \delta\right]\\
+ \tfrac{1}{2}\left(f_0'' + \tfrac{1}{4}K_0^2 f_0\right)\left[\delta^2 \ln\left(R + \sqrt{R^2+\delta^2}\right) - \delta^2 \ln \delta - \frac{\delta^2 R}{\sqrt{R^2+\delta^2}}\right].
\end{aligned}$$

Now the second half of the original integral is

$$I_2(\delta) = \delta^2 \int_{-\ell}^{0} \frac{f(t)}{(|\boldsymbol{r}(t)|^2+\delta^2)^{3/2}}\,dt = \delta^2 \int_{0}^{\ell} \frac{f(-t)}{(|\boldsymbol{r}(-t)|^2+\delta^2)^{3/2}}\,dt.$$

Using the same approach we conclude that

$$\begin{aligned} I_2(\delta) &= f_0 \frac{P}{\sqrt{P^2+\delta^2}} + f_0' \left[\frac{\delta^2}{\sqrt{P^2+\delta^2}} - \delta\right] \\ &\quad + \tfrac{1}{2}\big(f_0'' + \tfrac{1}{4}K_0^2 f_0\big)\left[\delta^2 \ln\big(P+\sqrt{P^2+\delta^2}\big) - \delta^2 \ln\delta - \frac{\delta^2 P}{\sqrt{P^2+\delta^2}}\right] + O(\delta^2), \end{aligned}$$

where $P = |\boldsymbol{r}(-\ell)|$.

Combining the results we have

$$\begin{aligned} I(\delta) &= f_0\left[\frac{R}{\sqrt{R^2+\delta^2}} + \frac{P}{\sqrt{P^2+\delta^2}} - \frac{2\ell}{\sqrt{\ell^2+\delta^2}}\right] + f_0'\left[\frac{\delta^2}{\sqrt{P^2+\delta^2}} - \frac{\delta^2}{\sqrt{R^2+\delta^2}}\right] \\ &\quad + \tfrac{1}{2}\big(f_0'' + \tfrac{1}{4}K_0^2 f_0\big)\Big[\delta^2 \ln\big(P+\sqrt{P^2+\delta^2}\big) + \delta^2 \ln\big(R+\sqrt{R^2+\delta^2}\big) \\ &\qquad - 2\delta^2 \ln\delta - \frac{\delta^2 P}{\sqrt{P^2+\delta^2}} - \frac{\delta^2 R}{\sqrt{R^2+\delta^2}}\Big] + O(\delta^2) \\ &= -\big(f_0'' + \tfrac{1}{4}K_0^2 f_0\big)\delta^2 \ln\delta + O(\delta^2). \end{aligned}$$

□

References

[1] J. Ainley, S. Durkin, R. Embid, P. Boindala, and R. Cortez, *The method of images for regularized Stokeslets*, J. Comput. Phys. **227** (2008), no. 9, 4600–4616. MR 2009e:76050 Zbl 05276040

[2] G. K. Batchelor, *An introduction to fluid dynamics*, Cambridge University Press, Cambridge, 1967. MR 2000j:76001 Zbl 0152.44402

[3] ———, *Slender-body theory for particles of arbitrary cross-section in Stokes flow*, J. Fluid Mech. **44** (1970), 419–440. MR 47 #1375 Zbl 0216.52401

[4] A. T. Chwang and T. Y. Wu, *A note on the helical movements of micro-organisms*, Proc. Roy. Soc. Lond. B **178** (1971), 327–346.

[5] R. Cortez, *A vortex/impulse method for immersed boundary motion in high Reynolds number flows*, J. Comput. Phys. **160** (2000), no. 1, 385–400. MR 2000m:76087 Zbl 0964.76067

[6] R. D. Dresdner and D. F. Katz, *Relationships of mammalian sperm motility and morphology to hydrodynamic aspects of cell function*, Biol. Reprod. **25** (1981), no. 5, 920–930.

[7] L. Fauci and A. McDonald, *Sperm motility in the presence of boundaries*, Bull. Math. Biol. **57** (1995), 679–699.

[8] L. J. Fauci and A. L. Fogelson, *Truncated Newton methods and the modeling of complex immersed elastic structures*, Comm. Pure Appl. Math. **46** (1993), no. 6, 787–818. MR 94e:92018 Zbl 0741.76103

[9] L. J. Fauci and C. S. Peskin, *A computational model of aquatic animal locomotion*, J. Comput. Phys. **77** (1988), no. 1, 85–108. MR 90e:92007 Zbl 0641.76140

[10] J. Gray and G. J. Hancock, *The propulsion of sea-urchin spermatozoa*, J. Exp. Biol. **32** (1955), no. 4, 802–814.

[11] S. Gueron and N. Liron, *Ciliary motion modeling, and dynamic multicilia ineractions*, Biophys. J. **63** (1992), 1045–1058.

[12] ———, *Simulations of three-dimensional ciliary beats and cilia interactions*, Biophys. J. **65** (1993), 499–507.

[13] R. E. Johnson and C. J. Brokaw, *A comparison between resistive-force theory and slender-body theory*, Biophys. J. **25** (1979), 113–127.

[14] R. E. Johnson and T. Y. Wu, *The asymptotic solution formula for uniform flow past a slender torus*, J. Fluid Mech. **95** (1979), 263–277.

[15] R. E. Johnson, *An improved slender-body theory for Stokes flow*, J. Fluid Mech. **99** (1980), no. 2, 411–431. MR 81g:76045 Zbl 0447.76037

[16] J. B. Keller and S. I. Rubinow, *Slender-body theory for slow viscous flow*, J. Fluid Mech. **75** (1976), 705–714.

[17] J. Lighthill, *Mathematical biofluiddynamics*, Regional Conference Series in Applied Mathematics, no. 17, Society for Industrial and Applied Mathematics, Philadelphia, 1975. MR 57 #9113 Zbl 0312.76076

[18] ———, *Flagellar hydrodynamics*, SIAM Rev. **18** (1976), no. 2, 161–230. MR 53 #2413 Zbl 0366.76099

[19] ———, *Helical distributions of Stokeslets: The centenary of a paper on slow viscous flow by the physicist h. a. lorentz*, J. Engrg. Math. **30** (1996), no. 1-2, 35–78. MR 97e:76099 Zbl 0883.76099

[20] M. J. Shelley and T. Ueda, *The Stokesian hydrodynamics of flexing, stretching filaments*, Phys. D **146** (2000), no. 1-4, 221–245. MR 2001j:74024 Zbl 1049.76016

[21] D. J. Smith, E. A. Gaffney, J. R. Blake, and J. C. Kirkman-Brown, *Human sperm accumulation near surfaces: a simulation study*, J. Fluid Mech. **621** (2009), 289–320. Zbl 1171.76476

[22] D. Smith, J. Blake, and E. Gaffney, *Fluid mechanics of nodal flow due to embryonic primary cilia*, J. R. Soc. Interface **5** (2008), 567–573.

[23] G. Taylor, *The action of waving cylindrical tails in propelling microscopic organisms*, Proc. Roy. Soc. London. Ser. A. **211** (1952), 225–239. MR 14,104e Zbl 0046.18904

[24] A.-K. Tornberg and M. J. Shelley, *Simulating the dynamics and interactions of flexible fibers in Stokes flows*, J. Comput. Phys. **196** (2004), no. 1, 8–40. MR 2004m:76164 Zbl 1115.76413

Received July 9, 2010. Revised August 29, 2011.

RICARDO CORTEZ: rcortez@tulane.edu
Mathematics Department, Tulane University, 6823 St. Charles Ave., New Orleans, LA 70118, United States
http://tulane.edu/sse/math/faculty/ricardo-cortez.cfm

MICHAEL NICHOLAS: mnichol@tulane.edu
Mathematics Department, Tulane University, 6823 St. Charles Ave., New Orleans, LA 70118, United States
http://faculty.carthage.edu/mnicholas

Communications in Applied Mathematics and Computational Science

map.berkeley.edu/camcos

See inside back cover or msp.berkeley.edu/camcos for submission instructions.

The subscription price for 2012 is US $75/year for the electronic version, and $105/year for print and electronic. Subscriptions, requests for back issues from the last three years and changes of subscribers address should be sent to Mathematical Sciences Publishers, Department of Mathematics, University of California, Berkeley, CA 94720-3840, USA.

Communications in Applied Mathematics and Computational Science, at Mathematical Sciences Publishers, Department of Mathematics, University of California, Berkeley, CA 94720-3840 is published continuously online. Periodical rate postage paid at Berkeley, CA 94704, and additional mailing offices.

CAMCoS peer review and production are managed by EditFLOW™ from Mathematical Sciences Publishers.

PUBLISHED BY
mathematical sciences publishers
http://msp.org/
A NON-PROFIT CORPORATION
Typeset in LaTeX

Communications in Applied Mathematics and Computational Science

vol. 7 no. 1 2012

1559-3940(2012)7:1;1-4